

ADformer: A Multi-Granularity Transformer for EEG-Based Alzheimer’s Disease Assessment

Yihe Wang, Nadia Mammone, Darina Petrovsky,
Alexandros T. Tzallas, Francesco C. Morabito, Xiang Zhang

Abstract—Electroencephalogram (EEG) has emerged as a cost-effective and efficient method for supporting neurologists in assessing Alzheimer’s disease (AD). Existing approaches predominantly utilize handcrafted features or Convolutional Neural Network (CNN)-based methods. However, the potential of the transformer architecture, which has shown promising results in various time series analysis tasks, remains underexplored in interpreting EEG for AD assessment. Furthermore, most studies are evaluated on the subject-dependent setup but often overlook the significance of the subject-independent setup. To address these gaps, we present *ADformer*, a novel multi-granularity transformer designed to capture temporal and spatial features to learn effective EEG representations. We employ multi-granularity data embedding across both dimensions and utilize self-attention to learn local features within each granularity and global features among different granularities. We conduct experiments across 5 datasets with a total of 525 subjects in setups including subject-dependent, subject-independent, and leave-subjects-out. Our results show that *ADformer* outperforms existing methods in most evaluations, achieving F1 scores of 75.19% and 93.58% on two large datasets with 65 subjects and 126 subjects, respectively, in distinguishing AD and healthy control (HC) subjects under the challenging subject-independent setup.

Index Terms—Alzheimer’s Disease, Dementia, EEG, Time Series, Transformers, Deep Learning

I. INTRODUCTION

Currently, over 55 million individuals worldwide suffer from various types of dementia, including Mild Cognitive Impairment (MCI), Frontotemporal Dementia (FTD), and Alzheimer’s disease (AD), which present a significant health challenge [1]. Among these, Alzheimer’s disease is the most common in the elderly population globally [2]. It is estimated that AD affects 10–30% of individuals over the age of 65, with an annual incidence rate of 1–3% [3]. While finding a cure for AD remains challenging, early assessment and intervention have proven to temporarily slow the progression of symptoms, potentially enhancing patients’ quality of life [4], [5]. However, AD assessment and diagnosis typically depend on expensive

medical infrastructure and specialist expertise, creating barriers in many poverty areas. Consequently, there is an urgent need for a straightforward and affordable assessment method. In contrast to neuroimaging techniques such as Magnetic Resonance Imaging (MRI) and Positron Emission Tomography (PET) [6], [7], electroencephalography (EEG) provides a non-invasive, portable, and cost-effective alternative for AD assessment, necessitating further exploration into this method [8], [9].

EEG is a type of medical time series data that captures brain activity, similar to how an electrocardiogram (ECG) records heart activity. It is typically collected using a medical helmet equipped with electrodes, and the data is multivariate, with each channel representing a specific region of brain activity [10]. Currently, two main research directions are employed to interpret EEG signals for AD assessment. The first direction utilizes traditional machine learning (ML) methods, which manually identify features such as statistical [11], [12], spectral [13], [14], power [15], [16], and complexity features [17], [18]. The second direction leverages modern deep-learning methods such as convolutional neural networks (CNN) [9], [19], [20], graph convolutional networks (GNN) [21], [22], and combinations of CNN and self-attention modules [23] are commonly used.

However, existing methods for EEG-based AD assessment have several limitations. Firstly, there is a notable absence of studies that utilize Transformer architectures specifically designed for this purpose. Given that EEG data is a type of time series with intricate dependencies across time points, the Transformer architecture, known for its superior capability to capture long-term dependencies, appears well-suited for EEG feature extraction and potentially offers advantages over traditional machine learning (ML) and convolutional neural network (CNN)-based methods in understanding EEG signals. Secondly, most current studies employ the subject-dependent setup, in which data is divided into training, validation, and test sets based on samples [9], [19]. There is a significant gap in research exploring the subject-independent setup [23], [24], where data is allocated based on subjects. Different setups could lead to significant discrepancies in results, potentially yielding deceptively high performance and limiting the model’s adaptability to real-world situations. Thirdly, the diversity and breadth of subjects and datasets examined in existing studies are limited. Most studies concentrate on a single EEG-AD dataset, typically using the 19-channel international standard setup collected during the subjects’ resting state. This situation underscores the need for more comprehensive research involving a broader range of subjects and datasets to evaluate the models’ applicability across various practical settings.

Yihe Wang and Xiang Zhang are with the Department of Computer Science, University of North Carolina - Charlotte, Charlotte, North Carolina 28223, United States.

Nadia Mammone and Francesco C. Morabito are with the DICEAM Department, University Mediterranea of Reggio Calabria Via Zehender, Feo di Vito, 89122 Reggio Calabria, Italy.

Darina Petrovsky is with the School of Nursing, Duke University, Durham, North Carolina 27708, United States.

Alexandros T. Tzallas is with the Department of Informatics & Telecommunications, University of Ioannina, Kostakioi, GR-47100, Arta, Greece.

Xiang Zhang is the corresponding author (E-mail: xiang.zhang@charlotte.edu). The code is available at <https://github.com/DL4mHealth/ADformer>

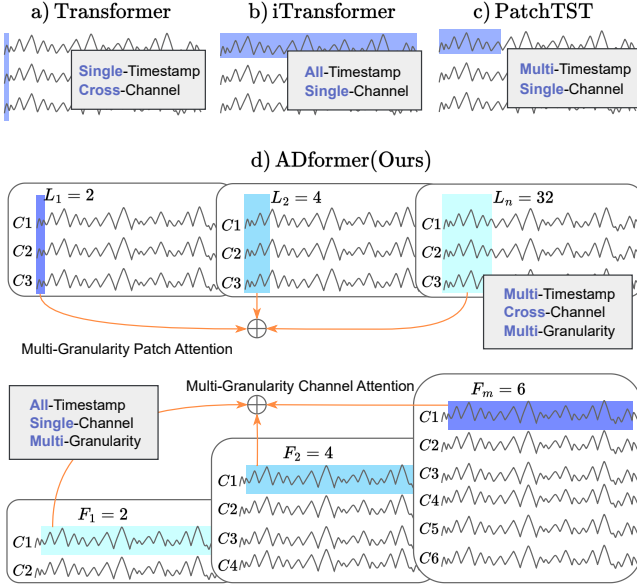


Fig. 1: **Token embedding methods.** Vanilla Transformer, Autoformer, and Informer [25]–[27] employ a single cross-channel timestamp as a token, while iTransformer [28] utilizes the whole series of a single channel as a token. PatchTST and Crossformer [29], [30] adopt a patch of timestamps from a single channel as a token. For ADformer, we propose one method that repetitively segments input into patches of varying lengths, each defined as one granularity, and embeds these cross-channel patches. Another method repetitively adjusts the number of channels in EEG data using 1-D convolutions, each specific target channel number defined as one granularity, and embeds the whole series of each channel.

To bridge these gaps, we introduce a multi-granularity transformer named *ADformer*, specifically tailored for EEG-based Alzheimer’s disease (AD) assessment. Our approach incorporates two novel data embedding methods along temporal and spatial dimensions: cross-channel multi-granularity patch embedding and whole-series multi-granularity channel embedding. The former method embeds cross-channel patches of varying lengths to explicitly capture temporal features across timestamps and implicitly gather spatial features among channels. Conversely, the latter method employs 1-D convolution to adjust the number of channels and embeds the entire series of a single channel, thereby explicitly capturing spatial features among channels and implicitly handling temporal features across timestamps. Figure 1 compares our embedding methods with existing data embedding methods used in time series transformers [25], [28], [29]. Moreover, we introduce two-stage intra-inter self-attention mechanisms: multi-granularity patch self-attention and multi-granularity channel self-attention, aligned with the two embedding strategies. The intra-granularity self-attention captures local features within each granularity, while the inter-granularity self-attention facilitates communication across different granularities. Additionally, We conduct experiments on five distinct datasets, involving a total of 525 subjects and 207,851 samples across binary and multi-class classification tasks with channel numbers of 7, 16, and 19. We

also assess four derived subsets of the large datasets ADFD and CNBPM, examining scenarios such as reduced class and channel numbers. We compare our approach with 19 baselines, including four traditional machine learning methods, four CNN-based methods, and 11 transformer-based methods. We perform extensive experimental setups, including subject-dependent, subject-independent, and leave-subjects-out setups. *ADformer* consistently outperforms many other models across various setups and datasets. For the challenging subject-independent setup, *ADformer* achieves F1 scores of 92.96% and 77.97% on the smaller datasets, ADSZ and APAVA, and 75.19% and 93.58% on the larger datasets, ADFD-Binary and CNBPM-Binary, respectively. We analyze all results under various setups, including performances of baseline methods, to identify factors contributing to the results across different setups.

We summarize our key contributions as follows:

- We introduce *ADformer*, a multi-granularity transformer specifically designed for EEG-based Alzheimer’s disease (AD) assessment.
- We present two novel data embedding methods to capture features along temporal and spatial dimensions, along with a two-stage intra-inter granularity self-attention mechanism that utilizes local features within each granularity and global features across different granularities.
- We conduct extensive experiments on five distinct datasets involving 525 subjects and 207,851 samples, including four derived subsets of two large datasets for case studies. We compare 19 baseline methods, including 4 traditional machine learning methods, 4 CNN-based methods, and 11 transformer-based methods, across various experimental setups such as subject-dependent, subject-independent, and leave-subjects-out scenarios.
- We thoroughly analyze the results of our method and the baselines to understand factors influencing performance across different experimental setups, discuss the limitations of current approaches, and suggest potential directions for future research on EEG-based Alzheimer’s disease (AD) assessment.

The rest of the paper is organized as follows: Section II reviews related works, including existing methods for EEG-based AD analysis and transformers in time series. Section III discusses preliminaries of experimental setups and their significance and defines the research problem. In Section IV, we detail the architecture of the proposed method. Section V provides information on the datasets used and implementation details. Section VI presents the results and their analysis for our method and all baselines under different experimental setups. Finally, we conclude the paper and suggest future works in Section VII.

II. RELATED WORK

A. EEG-based Alzheimer’s Disease Analysis

In EEG-based analysis for Alzheimer’s Disease (AD), there are two main research directions. The first direction involves identifying handcrafted features such as entropy, band-power, and spectral features, followed by employing standard classifiers like Multi-Layer Perceptron (MLP) and Support

Vector Machine (SVM) to differentiate these features. Examples include statistical features such as mean, skewness, kurtosis, standard deviation, max, min, and median [11], [12], [31]–[35]; spectral features such as phase shift, phase coherence, bispectrum, bicoherence, spectral centroid, spectral roll-off, spectral peak, average magnitude, median frequency, and amplitude modulation [13], [14], [36]–[40]; power features such as power spectrum density, relative band power, ratio of EEG rhythms, and energy [15], [16], [32], [41]; and complexity features such as Shannon entropy, Tsallis entropy, permutation entropy, spectral entropy, bispectral entropy, and dispersion entropy [17], [18], [42]–[44].

The second direction employs deep learning techniques to extract relevant features from EEG data automatically. For example, a study of [45] integrates a Restricted Boltzmann Machine (RBM) with an SVM classifier for EEG-based AD analysis. The method in [19] uses a CNN to extract dementia features and differentiate AD subtypes using an MLP. Additionally, some studies transform EEG data into images to characterize dementia features from frequency and energy perspectives. These include using power spectrum density (PSD) across channels and extracting spectrum energy features [9], transforming EEG sub-bands (theta, alpha, and beta) into 2D images [46], and converting EEG signals into time-frequency (TF) images with the short-time Fourier transform (STFT) for training with a 2D-CNN [20]. Moreover, some research efforts explore features across both timestamps and channels. For instance, introducing a spatial-temporal graph convolutional neural network (GCN) leverages the spatial topology of functional connectivity and dynamic temporal information [21] and enhancing node features with PSD similarity using gated graph convolution enables adaptive learning of graph structures [22]. Methods employing self-attention modules are also explored, such as DICE-Net, which combines PSD and Wavelet transform with a 2D-CNN and a self-attention module [23]. While most existing works employ a simple CNN model or a combination of CNN with a graph neural network or a self-attention module, pure transformer models utilizing state-of-the-art techniques or architectures remain under-explored. Importantly, most studies with deep learning methods evaluate the subject-dependent setup, with a notable lack of investigations into the challenging but practically significant subject-independent setting (Analysis in section III).

B. Transformer for Time Series

Time series transformers are primarily focused on three tasks: forecasting, classification, and anomaly detection. For classification, the Gated Transformer integrates two transformers to learn temporal and spatial information [47] simultaneously; ViTST converts time series data into images and employs a vision transformer for irregularly sampled time series [48]; Medformer utilizes cross-channel patching and intra-inter granularity self-attention for medical time series classification [49]. In anomaly detection, Memto introduces a novel method based on a memory-guided transformer [50]; Anomaly Transformer proposes an Anomaly-Attention mechanism to highlight discrepancies [51]. For forecasting, the Informer

designs ProbSparse attention to simplify self-attention and focuses on one-step forecasting [27]; Pyraformer uses a pyramidal attention module to enhance long-term dependency and streamline attention processes [52]; Autoformer replaces self-attention with auto-correlation and adds a decomposition feature for analyzing time series [26]. The Non-stationary Transformer adapts self-attention to manage non-stationary data [53]; FEDformer applies frequency domain insights to reform self-attention [54]; Crossformer, PatchTST, and CARD all employ patching techniques to improve feature learning [29], [30], [55], with Crossformer and CARD implementing self-attention across both time and channel dimensions. The iTransformer emphasizes the efficacy of channel-dimension self-attention in forecasting tasks [28]. Pathformer and Scaleformer utilize multi-granularity embedding to capture features at different scales, enabling models to learn fine-grained and coarse-grained patterns [56], [57].

III. PRELIMINARIES AND PROBLEM DEFINITION

A. EEG-Based Disease Assessment

EEG time series data, a type of medical time series, typically exhibits multiple data levels, including subject, session, trial, and sample levels [24]. In EEG data collected for disease diagnosis or assessment tasks, each subject usually receives a data label indicating the presence or absence of specific brain diseases, such as various types of dementia. It is also possible for multiple labels to be assigned to one subject if they have multiple diseases. Long sequences of time series data (Trial/Session) from each subject are often segmented into multiple shorter samples to enhance memory and computational efficiency for deep learning tasks. Consequently, each sample of EEG time series generally includes a class label indicating the disease type and a subject ID specifying its origin. Given the ultimate goal of diagnosing whether a subject has a particular disease, experimental setups must be meticulously designed to align with real-world medical applications. Diverse experimental setups can yield significantly different results, potentially leading to erroneous conclusions. Here, we introduce three widely employed setups in medical time series classification [9], [23], [49] and highlight their distinctions. Figure 2 adopted from [24] provides a simple illustration of two setups: subject-dependent and subject-independent.

B. Subject-Dependent

In this setup, the division into training, validation, and test sets is based on time series **samples**. All samples from various subjects are randomly shuffled and then allocated into the respective sets. Consequently, samples with identical subject IDs may be present in the training, validation, and test sets. This scenario potentially introduces “information leakage,” wherein the model could inadvertently learn the distribution specific to certain subjects during the training phase. This setup is typically employed for assessing whether a dataset exhibits cross-subject features and has limited applications under real-world medical time-series-based disease diagnosis scenarios. The reason is simple: we cannot know the label of unseen subjects and their corresponding samples during training. Generally, the results

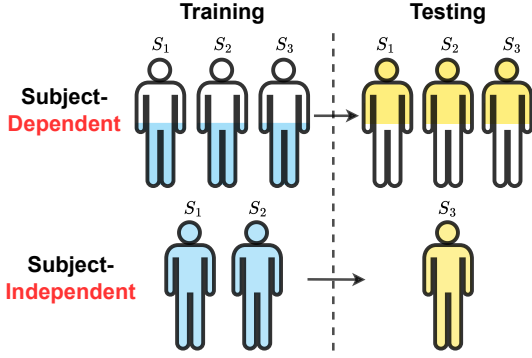


Fig. 2: **Subject-dependent/independent setups (Figure adopt from [24]).** In the subject-dependent setup, samples from the same subject can appear in both the training and test sets, causing information leakage. In the subject-independent setup, samples from the same subject are exclusively in either the training or test set, which is more challenging and practically meaningful but less studied.

of the subject-dependent setup tend to be notably higher than those from the subject-independent setup, often showing the upper limit of a dataset’s learning capability.

C. Subject-Independent

In this setup, the division into training, validation, and test sets is based on **subjects**. Each subject and their corresponding samples are exclusively distributed into one of the training, validation, or test sets. Consequently, samples with identical subject IDs can only be present in one of these sets. This setup holds significant importance in disease diagnosis tasks as it closely simulates real-world scenarios. It enables us to train a model on subjects with known labels and subsequently evaluate its performance on unseen subjects; in other words, evaluate if a subject has a specific disease. However, this setup poses significant challenges in medical time series classification tasks. Due to the variability in data distribution and the potential presence of unknown noise within each subject’s data, capturing general features across subjects becomes challenging [24], [58]–[60]. Even if subjects share the same label, the personal noise inherent in each subject’s data may obscure these common features. Developing a method that effectively captures common features among subjects while disregarding individual noise remains an unsolved problem.

D. Leave-Subjects-Out

This setup can be viewed as a variant of the subject-independent approach used in medical tasks [23]. Typically, medical data is both valuable and limited in quantity. To maximize the use of this data, researchers often leave several subjects (or just one, known as leave-one-out) as validation and test sets, while the remaining subjects are used to train the model. Researchers can either cycle through all the subjects or use a random seed to select different subjects as validation and test sets, computing average results across various seeds.

This setup is akin to a combination of k-fold validation and subject-independent methods, aiming to utilize all available data for training and testing to develop a robust model. Due to the inherent variance of subjects, the results usually suffer from high standard deviation.

E. Problem Definition

EEG-based Alzheimer’s Disease (AD) Assessment Consider an input EEG time series sample $x_{in} \in \mathbb{R}^{T \times C}$, where T represents the number of timestamps and C represents the number of channels. We aim to learn a representation h , which can be used to predict the corresponding label $y \in \mathbb{R}^K$. Here, K is the number of classes that have medical meanings, including labels such as Healthy Control (HC), Mild Cognitive Impairment (MCI), Alzheimer’s Disease(AD), and Frontotemporal Dementia (FTD).

IV. METHOD

A. Overview

Our method incorporates two branches to leverage features across temporal and spatial dimensions. The patch branch consists of a cross-channel multi-granularity patch embedding and multi-granularity patch self-attention for explicitly extracting temporal features and implicitly extracting spatial features. In contrast, the channel branch comprises a whole-series multi-granularity channel embedding and multi-granularity channel self-attention, explicitly extracting spatial features and implicitly extracting temporal features. The architecture of the proposed ADformer is depicted in Figure 3. The input time series data is transformed into augmented views for each granularity by randomly selecting augmentation methods from an augmentation bank. In the **cross-channel multi-granularity patch embedding**, we repeatedly segment the augmented views into patches of varying lengths, defined as different granularities, and embed these differently sized patches into patch embeddings. In the **whole-series multi-granularity channel embedding**, we perform dimension transformations to increase or decrease the channel numbers of the augmented views, also defined as different granularities, and then embed the entire series of each channel into channel embeddings. The **multi-granularity patch self-attention** and **multi-granularity channel self-attention** involve both intra and inter-granularity self-attention. The intra-granularity self-attention enables the model to identify intrinsic local features at different scales. Inter-granularity self-attention facilitates communication between different granularities through router mechanisms to learn global features. Inspired by contrastive learning, the augmentation step before data embedding encourages different granularities to learn mutual information and complement each other. Note that two branches are computed in parallel.

B. Augmentation Bank

Data augmentation is applied before data embedding to foster mutual information learning among different granularities during the inter-granularity self-attention stage. We select augmentation methods beneficial for time series classification

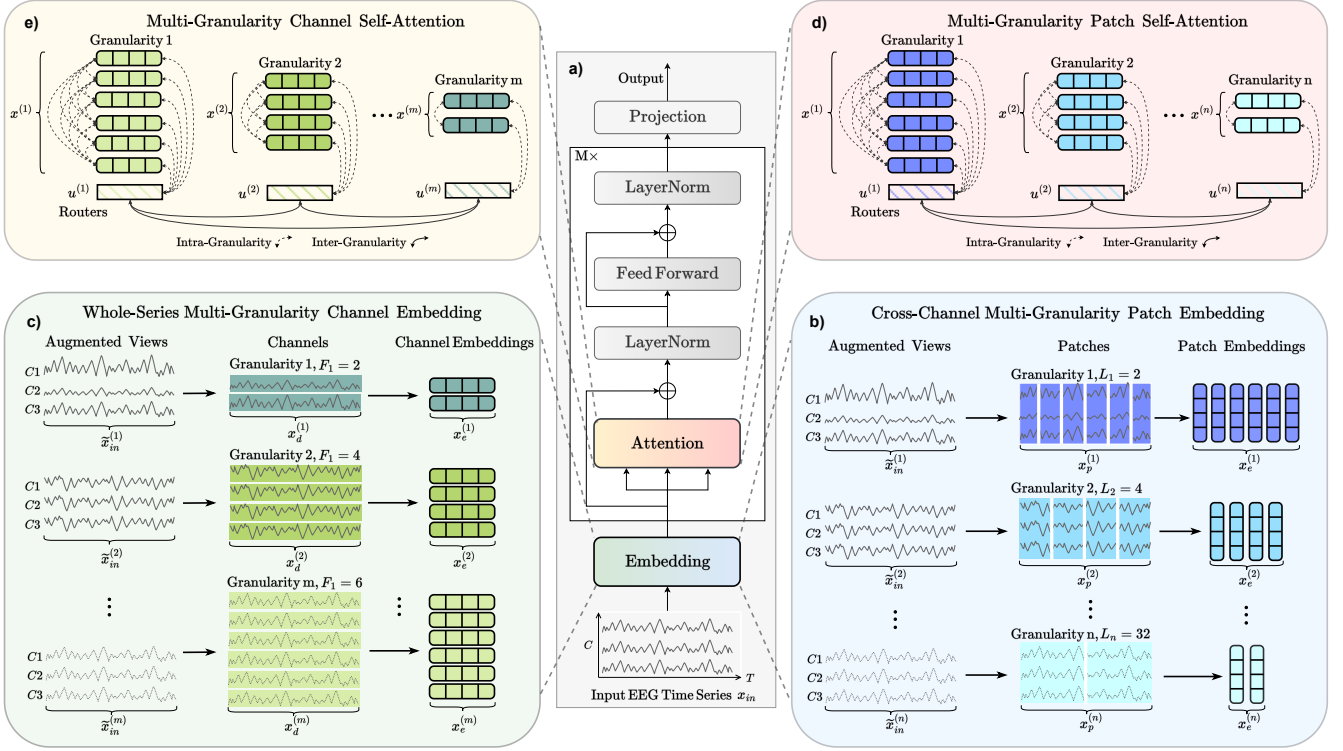


Fig. 3: **Overview of ADformer.** **a)** Workflow. **b)** For the i -th patch length L_i denoting granularity i and input sample x_{in} , we apply data augmentation to generate the augmented view $\tilde{x}_{in}^{(i)}$ and segment this view into cross-channel non-overlapping patches $x_p^{(i)}$. These patches are mapped into latent space and are combined with granularity and positional embeddings to produce the final patch embedding $x^{(i)}$. **c)** For the j -th target channel number F_j denoting granularity j and input sample x_{in} , we apply data augmentation to generate the augmented view $\tilde{x}_{in}^{(j)}$ and perform dimension transformation using 1-d convolution on the transposed augmented input $(\tilde{x}_{in}^{(j)})^T$ to adjust the number of channels. The entire series of channels are mapped into latent space and combined with the granularity embedding to produce the final channel embedding $x^{(j)}$. **d)** and **e)** We compute intra-granularity self-attention, which captures features within individual granularities, and inter-granularity self-attention, allowing for the exchange and learning of information across different granularities. A router mechanism is employed during inter-granularity self-attention to reduce time and space complexity.

tasks [24], [61], [62]. **(1) Temporal Flipping:** We reverse the EEG data along the temporal dimension. The likelihood of applying this augmentation is controlled by a parameter *prob*, with a default value of 0.5. **(2) Channel Shuffling:** We randomly shuffle the order of EEG channels. The probability of applying channel shuffling is controlled by the parameter *prob*, also set by default to 0.5. **(3) Frequency Masking:** First introduced in [63] for contrastive learning, this method involves converting the EEG data into the frequency domain, randomly masking some frequencies, and then converting it back. The proportion of frequencies masked is controlled by the parameter *ratio*, with a default value of 0.1. **(4) Jittering:** Random noise, ranging from 0 to 1, is added to the raw data. The intensity of the noise is adjusted by the parameter *scale*, which is set by default to 0.1. **(5) Drop Out:** Similar to the dropout layer in neural networks, this method randomly drops some values. The proportion of values dropped is controlled by the parameter *ratio*, with a default setting of 0.1.

C. Cross-Channel Multi-Granularity Patch Embedding

From a medical perspective, the brain functions as a cohesive unit, suggesting a naive assumption that there are inherent

correlations among different channels in EEG data [64]–[66]. *Motivated by the above assumption*, we reasonably propose cross-channel patching for token embedding, which is different from existing patch embedding methods that embed patches in a channel-independent manner and fail to capture inter-channel correlations [29], [30], [55]. Figure 1 provides an overview comparison of existing token embedding methods and ours. The upper part of our embedding method denotes cross-channel multi-granularity patch embedding. Additionally, the presence of EEG biomarkers hidden in certain frequency bands [15], [16], [41] further *motivates* us to employ multi-granularity patching. Unlike traditional methods such as up/downsampling or handcrafted band filtering, multi-granularity patching automatically simulates different frequency bands and captures band-related features.

Given the above rationales, we propose a novel token embedding approach: cross-channel multi-granularity patching. Given an input multivariate EEG sample $x_{in} \in \mathbb{R}^{T \times C}$, and a list of different patch lengths $\{L_1, L_2, \dots, L_n\}$. For the i -th patch length L_i denoting granularity i , we first apply data augmentations to obtain augmented views $\tilde{x}_{in}^{(i)} \in \mathbb{R}^{T \times C}$. Inspired by the contrastive learning framework [24], [67],

[68], we believe these augmentations enhance learning in the subsequent inter-granularity self-attention stage by encouraging different granularities to learn and complement information from each other.

We then segment the augmented view $\tilde{\mathbf{x}}_{\text{in}}^{(i)}$ into N_i cross-channel non-overlapping patches $\mathbf{x}_{\text{p}}^{(i)} \in \mathbb{R}^{N_i \times (L_i \cdot C)}$. Zero padding is applied to ensure that the number of timestamps T is divisible by L_i , making $N_i = \lceil T/L_i \rceil$. The patches are mapped into latent embeddings space using a linear projection: $\mathbf{x}_e^{(i)} = \mathbf{x}_{\text{p}}^{(i)} \mathbf{W}^{(i)}$, where $\mathbf{x}_e^{(i)} \in \mathbb{R}^{N_i \times D}$ and $\mathbf{W}^{(i)} \in \mathbb{R}^{(L_i \cdot C) \times D}$.

A fixed positional embedding $\mathbf{W}_{\text{pos}} \in \mathbb{R}^{G \times D}$ is generated for positional encoding [25], where G is a very large number. We add $\mathbf{W}_{\text{pos}}[1 : N_i] \in \mathbb{R}^{N_i \times D}$, the first N_i rows of the positional embedding \mathbf{W}_{pos} , along with a learnable granularity embedding $\mathbf{W}_{\text{gr}}^{(i)} \in \mathbb{R}^{1 \times D}$ for the i -th patch length L_i , to obtain the final patch embedding:

$$\mathbf{x}^{(i)} = \tilde{\mathbf{x}}_e^{(i)} + \mathbf{W}_{\text{pos}}[1 : N_i] + \mathbf{W}_{\text{gr}}^{(i)}, \quad (1)$$

where $\mathbf{x}^{(i)} \in \mathbb{R}^{N_i \times D}$. Note that the granularity embedding $\mathbf{W}_{\text{gr}}^{(i)}$ is broadcasted to all N_i embeddings during addition.

To facilitate communication among granularities and reduce time and space complexity, we initiate a router for the later multi-granularity patch self-attention:

$$\mathbf{u}^{(i)} = \mathbf{W}_{\text{pos}}[N_i + 1] + \mathbf{W}_{\text{gr}}^{(i)}, \quad (2)$$

where $\mathbf{u}^{(i)}$, $\mathbf{W}_{\text{pos}}[N_i + 1]$, $\mathbf{W}_{\text{gr}}^{(i)} \in \mathbb{R}^{1 \times D}$. Here, $\mathbf{W}_{\text{pos}}[N_i + 1]$ is utilized not for positional embedding but to inform the router about the number of patches at the current granularity L_i , and $\mathbf{W}_{\text{gr}}^{(i)}$ carries the granularity information. Both components help distinguish the routers from one another.

Finally, we obtain a list of patch embeddings $\{\mathbf{x}^{(1)}, \mathbf{x}^{(2)}, \dots, \mathbf{x}^{(n)}\}$ and router embeddings $\{\mathbf{u}^{(1)}, \mathbf{u}^{(2)}, \dots, \mathbf{u}^{(n)}\}$ corresponding to different patch lengths $\{L_1, L_2, \dots, L_n\}$. These embeddings are then fed into the two-stage multi-granularity patch self-attention.

D. Multi-Granularity Patch Self-Attention

Our goal is to learn multi-granularity features and allow granularity interactions during self-attention. A naive approach to achieve this is to concatenate all the patch embeddings $\{\mathbf{x}^{(1)}, \mathbf{x}^{(2)}, \dots, \mathbf{x}^{(n)}\}$ into a large patch embedding $\mathbf{X} \in \mathbb{R}^{(\sum_{i=1}^n N_i) \times D}$ and perform self-attention on this new embedding, where n denotes the number of different granularities. However, this approach leads to a time complexity of $O\left(\left(\sum_{i=1}^n N_i\right)^2\right)$, which is impractical for a large n .

To reduce the computational complexity, we introduce a router mechanism and divide the self-attention process into two distinct stages: a) intra-granularity and b) inter-granularity self-attention. The intra-granularity stage focuses on performing self-attention within the same granularity, allowing the model to capture the unique features of each granularity. Conversely, the inter-granularity stage facilitates self-attention across different granularities, promoting the learning of mutual information and enhancing the complementarity of features among granularities.

1) *Intra-Granularity Patch Self-Attention*: For the i -th patch length L_i denoting granularity i , we concatenate the patch embedding $\mathbf{x}^{(i)} \in \mathbb{R}^{N_i \times D}$ and router embedding $\mathbf{u}^{(i)} \in \mathbb{R}^{1 \times D}$ to form an intermediate sequence of embeddings $\mathbf{z}^{(i)} \in \mathbb{R}^{(N_i+1) \times D}$:

$$\mathbf{z}^{(i)} = \left[\mathbf{x}^{(i)} \parallel \mathbf{u}^{(i)} \right] \quad (3)$$

where $[\cdot \parallel \cdot]$ denotes concatenation. Self-attention is then performed on $\mathbf{z}^{(i)}$ for both the patch and router embeddings:

$$\begin{aligned} \mathbf{x}^{(i)} &\leftarrow \text{Attn}^{\text{Intra-t}} \left(\mathbf{x}^{(i)}, \mathbf{z}^{(i)}, \mathbf{z}^{(i)} \right) \\ \mathbf{u}^{(i)} &\leftarrow \text{Attn}^{\text{Intra-t}} \left(\mathbf{u}^{(i)}, \mathbf{z}^{(i)}, \mathbf{z}^{(i)} \right) \end{aligned} \quad (4)$$

where $\text{Attn}^{\text{Intra-t}}(\mathbf{Q}, \mathbf{K}, \mathbf{V})$ refers to the scaled dot-product attention mechanism described in [25]. The router embedding $\mathbf{u}^{(i)}$ is updated simultaneously with the patch embedding $\mathbf{x}^{(i)}$ to ensure consistency. This update allows the router embedding to summarize features at the current training step within the same granularity, while the patch embeddings receive global information from the router. The intra-granularity self-attention mechanism helps the model to capture features within the same granularity, facilitating the extraction of local features and correlations among timestamps of the same scale.

2) *Inter-Granularity Patch Self-Attention*: We concatenate all router embeddings $\{\mathbf{u}^{(1)}, \mathbf{u}^{(2)}, \dots, \mathbf{u}^{(n)}\}$ to form a sequence of routers $\mathbf{U}^t \in \mathbb{R}^{n \times D}$:

$$\mathbf{U}^t = \left[\mathbf{u}^{(1)} \parallel \mathbf{u}^{(2)} \parallel \dots \parallel \mathbf{u}^{(n)} \right] \quad (5)$$

where n is the number of different granularities. For each granularity i with patch length L_i , we apply self-attention to the router embedding $\mathbf{u}^{(i)} \in \mathbb{R}^{1 \times D}$ with all the routers \mathbf{U}^t :

$$\mathbf{u}^{(i)} \leftarrow \text{Attn}^{\text{Inter-t}} \left(\mathbf{u}^{(i)}, \mathbf{U}^t, \mathbf{U}^t \right) \quad (6)$$

This process allows each router, incorporating local information from its respective granularity through intra-granularity self-attention, to exchange and learn information across different granularities. This inter-granularity self-attention effectively captures features across various scales. Moreover, the router mechanism significantly reduces the time complexity compared to the naive approach, from $O\left(\left(\sum_{i=1}^n N_i\right)^2\right)$ to $O\left(\sum_{i=1}^n N_i^2 + n^2\right)$. Given that $N_i \leq T$, the worst-case time complexity for the two-stage multi-granularity patch self-attention becomes $O(nT^2 + n^2)$.

E. Whole-Series Multi-Granularity Channel Embedding

When discussing cross-channel patch embedding, this token embedding method implicitly learns channel correlations by embedding all channels together and applying self-attention to the temporal dimension. We could also explicitly leverage channel correlations by performing self-attention along the channel dimension. Existing work, such as the iTransformer [28], has demonstrated the effectiveness of embedding the entire series of a single channel as a token to learn effective representations. Moreover, as previously discussed, multi-granularity embedding

methods benefit from learning features at different scales. Could we also apply this technique to whole-series channel embedding?

Given these insights, we propose a novel token embedding method: whole-series multi-granularity channel embedding, which aims to represent the data better and capture complex channel interactions at various granularity levels. The lower part of our embedding method in Figure 1 illustrates this embedding method. Given an input multivariate EEG sample $\mathbf{x}_{\text{in}} \in \mathbb{R}^{T \times C}$, and a list of target channel number $\{F_1, F_2, \dots, F_m\}$. For the j -th target channel number F_j denoting granularity j , we first apply data augmentations to obtain augmented input $\tilde{\mathbf{x}}_{\text{in}}^{(j)} \in \mathbb{R}^{T \times C}$. Again, the data augmentation is intended to enhance learning during the inter-granularity self-attention stage by encouraging different granularities to learn mutual information.

We then perform dimension transformation using 1-d convolution to the transposed augmented input $(\tilde{\mathbf{x}}_{\text{in}}^{(j)})^T \in \mathbb{R}^{C \times T}$ to adjust the number of channels. For target channel number F_j , we obtain $\mathbf{x}_d^j \in \mathbb{R}^{F_j \times T}$, where a higher channel number F_j is defined as finer granularity, and a lower channel number as coarser granularity. From a medical perspective of EEG data, each channel represents activities from a specific brain region; the finer granularity of embedding extracts more latent information from raw data and better represents the whole brain. Then, the \mathbf{x}_d^j is further mapped into latent embeddings using a linear projection: $\mathbf{x}_e^{(j)} = \mathbf{x}_d^j \mathbf{W}^{(j)}$, where $\mathbf{x}_e^{(j)} \in \mathbb{R}^{F_j \times D}$ and $\mathbf{W}^{(j)} \in \mathbb{R}^{T \times D}$.

Positional embedding is unnecessary here since self-attention is performed along the channel dimension. We only add the learnable granularity embedding $\mathbf{W}_{\text{gr}}^{(j)} \in \mathbb{R}^{1 \times D}$ here to help distinguish the j -th granularity from others, resulting in the final channel embedding:

$$\mathbf{x}^{(j)} = \tilde{\mathbf{x}}_e^{(j)} + \mathbf{W}_{\text{gr}}^{(j)}, \quad (7)$$

where $\mathbf{x}^{(j)} \in \mathbb{R}^{F_j \times D}$. The granularity embedding $\mathbf{W}_{\text{gr}}^{(j)}$ is broadcasted to all F_j channels during addition. We also enable a router mechanism here to reduce complexity and facilitate inter-granularity self-attention later. The router embedding is initialized as:

$$\mathbf{u}^{(j)} = \mathbf{W}_{\text{gr}}^{(j)}, \quad (8)$$

where $\mathbf{u}^{(j)} \in \mathbb{R}^{1 \times D}$. Again, the granularity embedding $\mathbf{W}_{\text{gr}}^{(j)}$ is aimed to make different granularity distinguishable from each other.

Finally, we obtain a list of channel embeddings $\{\mathbf{x}^{(1)}, \mathbf{x}^{(2)}, \dots, \mathbf{x}^{(m)}\}$ and router embeddings $\{\mathbf{u}^{(1)}, \mathbf{u}^{(2)}, \dots, \mathbf{u}^{(m)}\}$ of different target channel numbers $\{F_1, F_2, \dots, F_m\}$. We feed the embeddings to the two-stage multi-granularity channel self-attention.

F. Multi-Granularity Channel Self-Attention

Like multi-granularity patch self-attention, we enable a router mechanism to facilitate communication among granularities and reduce complexity in multi-granularity channel self-attention. This process is divided into intra-granularity and

inter-granularity self-attention stages. In the intra-granularity stage, self-attention is performed within the same granularity among channel tokens to capture channel-wise correlations. In the inter-granularity stage, self-attention is performed across different granularities to enforce mutual information learning between them.

1) *Intra-Granularity Channel Self-Attention*: For the j -th target channel number F_j denoting granularity j , we concatenate the channel embedding $\mathbf{x}^{(j)} \in \mathbb{R}^{F_j \times D}$ and the router embedding $\mathbf{u}^{(j)} \in \mathbb{R}^{1 \times D}$ to form an intermediate embedding $\mathbf{z}^{(j)} \in \mathbb{R}^{(F_j+1) \times D}$:

$$\mathbf{z}^{(j)} = [\mathbf{x}^{(j)} \parallel \mathbf{u}^{(j)}] \quad (9)$$

where $[\cdot \parallel \cdot]$ denotes concatenation. We perform self-attention on the new $\mathbf{z}^{(j)}$ for both the channel embedding $\mathbf{x}^{(j)}$ and the router embedding $\mathbf{u}^{(j)}$:

$$\begin{aligned} \mathbf{x}^{(j)} &\leftarrow \text{Attn}^{\text{Intra-c}}(\mathbf{x}^{(j)}, \mathbf{z}^{(j)}, \mathbf{z}^{(j)}) \\ \mathbf{u}^{(j)} &\leftarrow \text{Attn}^{\text{Intra-c}}(\mathbf{u}^{(j)}, \mathbf{z}^{(j)}, \mathbf{z}^{(j)}) \end{aligned} \quad (10)$$

where $\text{Attn}(\mathbf{Q}, \mathbf{K}, \mathbf{V})$ denotes the scaled dot-product attention mechanism in [25]. Again, the router embedding $\mathbf{u}^{(j)}$ is updated simultaneously with the channel embedding $\mathbf{x}^{(j)}$ to maintain consistency. This ensures that the router can summarize channel correlations within the same granularity while the channel embeddings receive global information from the router. The intra-granularity self-attention mechanism enables the model to capture channel correlations within the same granularity, facilitating the extraction of local features at that granularity.

2) *Inter-Granularity Channel Self-Attention*: We concatenate all router embeddings $\{\mathbf{u}^{(1)}, \mathbf{u}^{(2)}, \dots, \mathbf{u}^{(m)}\}$ to form a sequence of routers $\mathbf{U}^c \in \mathbb{R}^{m \times D}$:

$$\mathbf{U}^c = [\mathbf{u}^{(1)} \parallel \mathbf{u}^{(2)} \parallel \dots \parallel \mathbf{u}^{(m)}] \quad (11)$$

where m is the number of different granularities. For granularity j with target channel number F_j , we apply self-attention to the router embedding $\mathbf{u}^{(j)} \in \mathbb{R}^{1 \times D}$ with all the routers \mathbf{U}^c :

$$\mathbf{u}^{(j)} \leftarrow \text{Attn}^{\text{Inter-c}}(\mathbf{u}^{(j)}, \mathbf{U}^c, \mathbf{U}^c) \quad (12)$$

Through intra-granularity self-attention, each router contains local information specific to a particular granularity. By performing self-attention among routers, the information can be exchanged and learned across different granularities, effectively capturing features more robustly. By using the router mechanism, the time complexity of the two-stage multi-granularity channel self-attention is $O\left(\sum_{j=1}^n F_j^2 + m^2\right)$.

G. Summary

Our method employs the standard Transformer architecture depicted in Figure 1. The two embedding techniques, shown in areas b) and c), are computed in parallel, as are the two self-attention mechanisms in areas d) and e). Both the

TABLE I: **Processed Data.** The information for the processed datasets is presented in two tables. The first table shows the confidentiality level, number of subjects, samples, classes, channels, sampling rate, sample timestamps, and file size. Here, **#-Timestamps** indicates the number of timestamps per sample. The second table shows the number of samples allocated to the training, validation, and test sets under different setups, including subject-dependent, subject-independent, and leave-subjects-out. The symbol - indicates no data, signifying that we do not evaluate this dataset under the specified setup, and the symbol \sim indicates the approximate number.

Dataset Name	Confidentiality Level	#-Subject	#-Sample	#-Class	#-Channel	#-Timestamps	Sampling Rate	File Size
ADSZ	Public	24+24=48	768	2	19	128	128Hz	14.2MB
APAVA	Public	12+11=23	5,967	2	16	256	256Hz	103MB
ADFD	Public	36+23+29=88	69,752	3	19	256	256Hz	2.52GB
ADFD-Binary	Public	36+29=65	53,182	2	19	256	256Hz	1.92GB
ADFD-Binary-7C	Public	36+29=65	69,752	2	7	256	256Hz	\sim 724MB
CNBPM	Private	63+63+63=189	70,064	3	19	256	256Hz	2.53GB
CNBPM-Binary	Private	63+63=126	46,305	2	19	256	256Hz	1.36GB
CNBPM-Binary-7C	Private	63+63=189	46,305	2	7	256	256Hz	\sim 513MB
Cognition-ERP	Private	90+87=177	61,300	2	7	149	125Hz	487MB

Dataset Name	Subject-Dependent			Subject-Independent			Leave-Subjects-Out		
	#-Training	#-Validation	#-Test	#-Training	#-Validation	#-Test	#-Training	#-Validation	#-Test
ADSZ	460	154	154	420	166	182	-	-	-
APAVA	3,579	1,194	1,194	3,123	1,431	1,413	-	-	-
ADFD	41,850	13,951	13,951	40,446	14,658	14,648	-	-	-
ADFD-Binary	-	-	-	31,294	10,416	11,472	\sim 40,000	\sim 6,500	\sim 6,500
ADFD-Binary-7C	-	-	-	31,294	10,416	11,472	-	-	-
CNBPM	42,038	14,013	14,013	37,389	15,361	17,314	-	-	-
CNBPM-Binary	-	-	-	25,438	9,990	10,877	\sim 32,000	\sim 7,500	\sim 6,500
CNBPM-Binary-7C	-	-	-	25,438	9,990	10,877	-	-	-
Cognition-ERP	36,780	12,260	12,260	35,100	13,200	13,000	-	-	-

patch embedding and channel embedding branches include their respective layer norm and feed-forward layers, and the computations for each are performed concurrently. Each branch shares layer normalization and feedforward networks across different granularities, which saves memory and computing resources.

For a given sample x_{in} , after M layers of self-attention processing, we obtain a list of updated patch embeddings $x^{(1)}, x^{(2)}, \dots, x^{(n)}$, and a list of channel embeddings $x^{(1)}, x^{(2)}, \dots, x^{(m)}$. We then concatenate these embeddings to form a final representation h , which is used to predict the label $y \in \mathbb{R}^K$ using a projection layer in downstream classification tasks. Note that although we discuss multi-granularity here, our method is flexible and can be easily adapted to variants such as single-granularity, repetitive granularities, or using only one of the embedding branches: patch or channel.

V. EXPERIMENTAL SETUPS

A. Datasets

To evaluate the performance of our method, we utilize 5 raw EEG Dementia datasets: ADSZ [69], APAVA [70], ADFD [71], CNBPM [72], [73], and Cognition-ERP [74], which include three public and two private datasets. The ADSZ, APAVA, ADFD, and CNBPM are resting EEG data, while Cognition-ERP is event-related potential data. These datasets include types of dementia such as Mild Cognitive Impairment (MCI), Frontotemporal Dementia (FTD), and Alzheimer’s Disease (AD). Altogether, these datasets comprise 525 distinct subjects and a total of 207,851 samples. One dataset has 7 channels, another 16 channels, and the remaining three have 19 channels.

Additionally, we use subsets of ADFD and CNBPM for more case studies by removing subjects with specific classes or reducing channel utilization, which generates 4 derived datasets: ADFD-Binary, ADFD-Binary-7C, CNBPM-Binary, and CNBPM-Binary-7C. The first tabular in table I presents the details of 9 processed datasets. For more details of raw data and data processing steps, see Appendix S.I.

B. Implementation Details

The differences and importance of the three evaluation setups are discussed in Section III. For the **subject-dependent** setup, after randomly shuffling the samples using seed 42, we divided them into training, validation, and test sets, allocating 60%, 20%, and 20% of total samples, respectively. Five processed datasets, including ADSZ, APAVA, ADFD, CNBPM, and Cognition-ERP, are evaluated under this setup. For the **subject-independent** setup, all the processed datasets are utilized, and the sample allocation strategy varies by dataset. For the ADSZ, ADFD, ADFD-Binary, ADFD-Binary-7C, and Cognition-ERP datasets, we distributed 60%, 20%, and 20% of the subjects and their corresponding samples into the training, validation, and test sets. Notice that for the CNBPM, CNBPM-Binary, and CNBPM-Binary-7C datasets, we randomly shuffle the subjects before splitting due to fewer samples from the final 20% of subjects in the raw order. For the APAVA dataset, we specifically allocated samples from subjects with IDs 1, 2, 17, and 18 to the validation set and those from subjects with IDs 15, 16, 19, and 20 to the test set, with the remaining samples going to the training set. For **leave-subjects-out**, we only evaluate on ADFD-Binary and CNBPM-Binary datasets. For ADFD-Binary,

TABLE II: **Subject-Dependent: All Complete Datasets.** The results of using the subject-dependent setup are presented here. The training, validation, and test sets are divided based on samples that have been randomly shuffled and then allocated according to predetermined ratios. More details about this setup can be found in Section III-B. For reference, the number of classes, channels, and subjects for each dataset is listed under the dataset name. The first tabular in Table I provides more details about each dataset.

Metrics Models	ADSZ (2 Classes, 19 Channels) (48 Subjects)		APAVA (2 Classes, 19 Channels) (23 Subjects)		ADFD (3 Classes, 19 Channels) (88 Subjects)		CNBPM (3 Classes, 19 Channels) (189 Subjects)		Cognision-ERP (2 Classes, 7 Channels) (177 Subjects)	
	Accuracy	F1 Score	Accuracy	F1 Score	Accuracy	F1 Score	Accuracy	F1 Score	Accuracy	F1 Score
Statistical	91.56±1.42	91.56±1.42	98.44±0.40	98.37±0.42	61.22±0.76	57.45±0.92	68.12±0.40	62.16±0.75	65.46±0.45	65.38±0.46
Spectral	98.18±0.86	98.18±0.86	99.38±0.23	99.35±0.24	61.01±1.11	57.94±1.07	70.75±0.45	67.46±0.33	66.15±0.14	66.07±0.15
Power	93.38±1.32	93.37±1.33	98.56±0.17	98.49±0.18	59.13±2.06	56.79±1.58	69.07±0.62	65.85±0.69	61.78±1.08	61.48±0.84
Complexity	91.95±1.95	91.94±1.96	96.85±0.42	96.71±0.44	47.52±1.55	43.80±1.54	57.21±1.27	52.32±1.06	56.42±0.83	56.18±0.71
EEGNet	91.17±2.16	91.16±2.17	99.46±0.19	99.44±0.20	80.79±0.71	78.99±1.13	86.18±0.51	84.03±0.57	72.11±0.19	72.00±0.18
TCN	98.05±0.82	98.05±0.82	99.28±0.34	99.25±0.35	81.39±0.46	80.33±0.37	85.51±0.25	83.25±0.22	73.06±0.21	72.96±0.12
MICN	69.22±4.04	69.18±4.06	98.96±0.25	98.91±0.26	76.13±0.44	75.09±0.33	82.17±0.37	79.53±0.33	68.52±0.28	68.32±0.27
TimesNet	98.31±0.88	98.31±0.88	99.82±0.11	99.81±0.12	93.74±0.62	93.52±0.62	91.20±0.37	89.93±0.41	75.59±0.41	75.50±0.40
Autoformer	95.71±2.45	95.71±2.45	98.91±0.36	98.87±0.38	87.83±1.62	87.38±1.79	81.29±4.44	78.41±5.01	70.64±0.80	70.55±0.85
Crossformer	87.14±87.14	87.07±2.73	97.07±0.18	96.94±0.19	89.35±1.32	88.88±1.40	88.38±0.92	86.59±1.07	68.30±0.36	68.09±0.37
FEDformer	91.82±1.46	91.81±1.47	93.55±0.38	93.24±0.41	77.63±2.37	76.60±2.46	77.98±0.62	74.67±0.74	66.35±0.44	66.22±0.54
Informer	95.45±0.71	95.45±0.71	99.03±0.33	98.99±0.34	90.93±0.90	90.60±0.94	88.42±0.37	86.80±0.39	76.10±0.57	75.99±0.59
iTransformer	81.43±2.48	81.24±2.57	92.50±0.52	92.19±0.56	64.90±0.25	62.25±0.33	71.17±0.47	66.15±0.45	66.13±0.29	66.06±0.29
MTST	88.96±1.42	88.96±1.42	98.58±0.32	98.52±0.33	65.08±0.69	63.03±0.58	73.35±0.51	69.87±0.63	67.91±0.17	67.83±0.17
Nonformer	97.14±0.32	97.14±0.32	99.51±0.06	99.49±0.07	96.12±0.47	95.96±0.47	92.86±0.45	91.77±0.55	77.46±0.64	77.35±0.64
PatchTST	89.87±1.67	89.87±1.68	97.76±0.54	97.66±0.56	66.26±0.40	64.95±0.42	73.92±0.49	70.30±0.33	68.84±0.40	68.79±0.41
Pyraformer	97.14±0.88	97.14±0.88	98.91±0.23	98.86±0.24	94.81±0.77	94.57±0.81	91.83±0.24	90.52±0.37	67.87±5.63	67.49±6.16
Reformer	97.01±1.13	97.01±1.13	99.30±0.23	99.27±0.24	91.51±1.75	91.14±1.83	88.71±0.48	87.08±0.53	75.49±0.30	75.40±0.30
Transformer	97.14±0.52	97.14±0.52	99.18±0.19	99.14±0.20	97.00±0.43	96.86±0.44	93.27±0.20	92.25±0.25	77.62±0.46	77.48±0.44
ADformer (Ours)	98.31±1.08	98.31±1.08	99.73±0.07	99.72±0.07	97.95±0.15	97.84±0.15	94.13±0.82	93.21±0.91	77.94±0.67	77.87±0.67

based on the current random seed, we randomly select 4 AD (Alzheimer’s Disease) and 4 HC (Healthy Controls) subjects for the validation set, and another 4 AD and 4 HC subjects for the test set; all remaining subjects are allocated to the training set. In the CNBPM-Binary dataset, this number increases to 10 AD and 10 HC subjects each for both the validation and test sets. These varying allocation ratios aim to maintain a balanced distribution of samples across the training, validation, and test sets. The detailed numbers of samples for each dataset under different setups are provided in the second tabular of Table I. All samples were normalized to standardize the channel data.

We compare our ADformer with 19 widely-used or state-of-art models, which include: 1) 4 traditional machine learning methods categorized in the review [8]: Statistical Features (Mean, Skewness, Kurtosis, Standard Deviation, Interquartile Range, Maximum, Minimum, and Median) [11], [12], [31]–[35], Spectral Features (Phase Shift, Phase Coherence, Bispectrum, Bicoherence, Spectral Centroid, Spectral Roll-off, Spectral Peak, Average Magnitude, Median Frequency, and Amplitude Modulation) [13], [14], [36]–[40], Power Features (Power Spectrum Density, Relative Band Power, Ratio of EEG Rhythm, and Energy) [15], [16], [32], [41], and Complexity Features (Shannon entropy, Tsallis Entropy, Permutation Entropy, Spectral Entropy, Bispectral Entropy, and Dispersion entropy) [17], [18], [42]–[44]; 2) 4 CNN-based methods: EEGNet [75], TCN [76], MICN [77], TimesNet [78]; and 3) 11 transformer-based methods: Autoformer [26], Crossformer [30], FEDformer [54], Informer [27], iTransformer [28], MTST [79], Nonformer [53], PatchTST [29], Pyraformer [52], Reformer [80], and Vanilla Transformer [25].

All CNN and transformer-based methods are implemented

based on the Time-Series-Library GitHub project¹. All traditional methods are manually implemented, and training is done under the same framework as deep-learning methods. We use accuracy, macro-averaged F1 score, macro-averaged AUROC, and macro-averaged AUPRC as evaluation metrics. For all the setups, we save the model with the best F1 score on the validation set and test it on the test set to get the final result. Experiments are conducted using five different seeds (41–45) based on the same train-val-test data split in subject-dependent/subject-independent setups and different train-val-test data split in the leave-subjects-out setup, with results reported as mean and standard deviation. Half of the experiments are performed on NVIDIA RTX 4090, and the other half that require more CUDA memory are run on a cluster with four RTX A5000 GPUs. We employ 6 layers for the encoder of all transformer methods, with the self-attention dimension D set to 128 and the hidden dimension of the feed-forward networks set to 256. The optimizer used is Adam, with a learning rate of $1e-4$. Stochastic weight averaging (SWA) [81] is enabled in subject-independent and leave-subjects-out setups to benefit cross-subjects learning. Batch size is set to $\{32, 32, 128, 128, 32\}$ to ADSZ, APAVA, ADFD, CNBPM, and Cognision-ERP, respectively. More implementation details and method-specific parameters, such as patch length list, are presented in the Supplement Materials S.II and the script files in our project’s GitHub repository.

TABLE III: **Subject-Independent: All Complete Datasets.** The results of using the subject-independent train-validation-test split are presented here. In this setup, the training, validation, and test sets are divided based on subjects, ensuring that samples from a single subject appear exclusively in one of the three sets. More details about this setup can be found in Section III-C. For reference, the number of classes, channels, and subjects for each dataset is listed under the dataset name. More details about each dataset are in the Table I.

Datasets	ADSZ (2 Classes, 19 Channels) (48 Subjects)		APAVA (2 Classes, 19 Channels) (23 Subjects)		ADFD (3 Classes, 19 Channels) (88 Subjects)		CNBPM (3 Classes, 19 Channels) (189 Subjects)		Cognition-ERP (2 Classes, 7 Channels) (177 Subjects)	
	Accuracy	F1 Score	Accuracy	F1 Score	Accuracy	F1 Score	Accuracy	F1 Score	Accuracy	F1 Score
Statistical	76.26±2.56	76.14±2.61	78.73±2.23	76.05±2.86	49.31±0.60	43.84±0.43	57.14±0.30	49.08±0.78	56.11±0.29	56.07±0.32
Spectral	87.58±1.72	87.36±1.69	74.48±0.57	69.42±0.97	43.16±3.28	41.43±2.30	56.01±1.59	51.86±0.77	54.87±0.34	54.71±0.34
Power	83.74±2.19	83.23±2.36	72.63±3.42	66.77±5.00	44.28±3.43	41.55±2.07	54.60±2.44	50.67±3.56	52.22±0.83	51.67±1.38
Complexity	81.43±2.77	81.11±2.87	66.83±5.57	60.99±7.22	37.05±3.43	36.91±2.93	46.91±0.95	43.19±1.43	52.03±1.31	51.08±2.70
EEGNet	86.81±1.84	86.65±1.91	71.81±3.67	65.26±5.86	51.78±0.93	47.49±0.85	66.69±0.32	60.02±0.61	56.30±0.52	56.04±0.55
TCN	88.90±0.64	88.80±0.62	84.71±1.25	83.69±1.25	50.17±1.37	47.29±1.30	66.19±0.35	60.38±0.55	54.11±0.58	53.73±0.89
MICN	60.55±2.01	60.49±2.04	79.45±1.81	75.93±2.61	47.00±2.01	43.43±1.25	65.04±1.12	60.02±0.80	54.65±0.23	54.56±0.33
TimesNet	92.75±1.57	92.65±1.56	76.30±4.02	72.89±5.34	48.81±1.12	47.69±1.04	67.81±1.35	62.40±1.98	52.97±1.06	52.60±1.10
Autoformer	91.43±4.63	91.36±4.60	68.64±1.82	68.06±1.94	45.25±1.48	42.59±1.85	61.25±2.32	56.60±3.25	53.86±0.30	53.72±0.33
Crossformer	84.51±2.47	84.39±2.40	73.77±1.95	68.93±1.85	50.45±2.31	45.50±1.70	59.76±1.56	51.42±2.66	55.71±0.80	55.45±0.95
FEDformer	90.44±2.90	90.37±2.88	74.94±2.15	73.51±3.39	46.30±0.59	43.91±1.37	62.48±0.70	56.95±0.96	55.29±0.59	55.18±0.68
Informer	90.22±1.53	90.12±1.53	73.11±4.40	69.47±5.06	48.45±1.96	45.74±1.38	63.42±1.79	58.35±1.45	50.39±0.59	50.28±0.46
iTransformer	78.79±1.72	78.60±1.65	74.55±1.66	72.30±1.79	52.60±1.59	46.79±1.13	58.42±0.55	48.89±0.67	55.31±0.76	55.29±0.75
MTST	76.15±3.49	76.09±3.47	71.14±1.59	64.01±3.16	45.60±2.03	44.31±1.74	54.34±2.02	49.43±1.35	54.41±0.67	53.81±0.79
Nonformer	90.44±0.82	90.36±0.79	71.89±3.81	69.74±3.84	49.95±1.05	46.96±1.35	70.36±1.79	65.78±2.19	50.95±1.08	50.66±1.12
PatchTST	79.12±1.97	78.09±2.36	67.03±1.65	55.97±3.10	44.37±0.95	41.97±1.37	58.02±1.67	51.83±1.66	53.12±0.30	53.05±0.32
Pyraformer	90.77±1.22	90.62±1.19	79.54±1.30	76.36±2.05	51.52±0.77	47.13±1.95	69.23±0.46	64.26±0.39	52.72±0.25	52.65±0.27
Reformer	89.56±1.87	89.48±1.86	78.70±2.00	75.93±1.82	50.78±1.17	47.94±0.69	66.11±1.29	61.47±1.79	52.58±0.54	52.40±0.48
Transformer	89.45±2.24	89.39±2.21	76.30±4.72	73.75±5.38	50.47±2.14	48.09±1.59	67.60±2.44	62.18±3.30	50.22±0.67	49.57±0.99
ADformer (Ours)	93.08±1.43	92.96±1.43	80.00±2.52	77.97±2.46	55.21±0.54	51.97±0.88	70.58±0.92	65.85±1.28	56.70±0.38	56.66±0.36

VI. EXPERIMENTAL RESULTS

A. Subject-Dependent

In this setup, we randomly shuffle all the subjects' samples and divide them into training, validation, and test sets according to a predetermined ratio. A more detailed discussion of this setup can be found in the preliminary section III-B. After splitting, the number of samples for each dataset is listed in the second tabular in Table I. The subject-dependent setup is designed to verify the effectiveness of a dataset and assess its cross-subject features. However, its real-world applications in EEG-based dementia diagnosis are limited, as the label of an unseen subject is unknown during the training phase. Typically, the results of this setup are much better than the subject-independent setup, showing the potential upper bound results achievable of a dataset with the subject-independent setup.

1) *All Complete Datasets:* We evaluated our ADformer and all baselines across five complete datasets: ADSZ, APAVA, ADFD, CNBPM, and Cognition-ERP. Table II presents the overall results under this setup. Our method achieves comparable or superior performance to the baselines in terms of accuracy and F1 score. Deep-learning methods demonstrate significantly stronger learning capabilities than traditional methods, especially on the larger datasets ADFD and CNBPM. The overall results indicate the presence of learnable features associated with different types of dementia across all datasets. Many methods, such as TimesNet, Nonformer, Pyraformer, and Transformer, can easily achieve over 90% F1 performance on various datasets. We hope the results under the

subject-dependent setup provide a clear impression to future researchers of how different setups could yield deceptively high performance, leading to training models that are ineffective in real-world applications. We aim to draw the attention of time series researchers to the significant challenges posed by the subject-independent setup in EEG-based disease diagnosis.

B. Subject-Independent

In this setup, we exclusively divide all subjects and their corresponding samples into training, validation, and test sets based on a predetermined ratio or specific subject IDs. The preliminary section III-C provides a more detailed discussion of this setup. After the division, the number of samples for each dataset is displayed in the second table in Table I. The outcomes of this setup are crucial as they reflect real-world applicability. For dementia diagnosis, it is essential to have a model that performs well on samples from unseen subjects to assess whether these subjects have dementia accurately. In this context, the labeled samples from these unseen subjects must not appear during the training phase (note that in some scenarios, unlabeled samples from unseen subjects might be used during training for domain adaptation, which is beyond the scope of our paper and is not discussed further). The unique distribution and noise inherent in each subject's data can obscure generalizable features across subjects, making it challenging to develop a model that performs well on unseen subjects. Typically, the subject-independent setup results are significantly worse than those from the subject-dependent setup.

1) *All Complete Datasets:* We evaluated our method and all baselines across five complete datasets: ADSZ, APAVA, ADFD, CNBPM, and Cognition-ERP. Table III presents the overall

¹<https://github.com/thuml/Time-Series-Library>

results under this setup. Our method achieves top-1 results in 8 out of 10 evaluations and top-2 in all 10 evaluations. For the relatively small datasets ADSZ and APAVA, CNN-based methods achieve comparable or even better results than transformer-based methods, which is intuitive. TCN achieves the best F1 score on APAVA. For the larger datasets, ADFD and CNBPM, the best and second-best results are all achieved by transformer-based methods. However, the overall performance on these two large datasets is not very impressive, with even the best results only reaching an F1 score of around 50% on a three-class classification task. On the Cognision-ERP dataset, all methods perform poorly, considering it is a binary classification task, achieving no more than 60% F1 scores with all methods. In general, deep-learning methods, including CNNs and transformers, easily outperform traditional methods, especially on the larger datasets ADFD and CNBPM.

The relatively low performance of ADFD and CNBPM prompts further investigation into potential causes. One possibility is that some classes of dementia, such as FTD and MCI, are challenging to distinguish from AD. Additionally, we are exploring the reasons behind the lower performance of the Cognision-ERP dataset, which may be attributed to the characteristics of ERP-EEG data or could be due to a fewer number of channels in the Cognision-ERP data. These insights lead to our focus on binary classification tasks for large datasets and channel reduction research in the upcoming sections.

TABLE IV: **Subject-Independent: Binary Classification of Large Datasets.** Subjects and their corresponding samples with an intermediate level of dementia, specifically Frontotemporal Dementia (FTD) and Mild Cognitive Impairment (MCI), are excluded from the datasets ADFD and CNBPM, respectively. We analyze the binary classification between Alzheimer’s Disease (AD) and Healthy Controls (HC) in these two large datasets, employing a subject-independent setup.

Datasets	ADFD-Binary (2 Classes, 19 Channels) (65 Subjects)		CNBPM-Binary (2 Classes, 19 Channels) (126 Subjects)	
	Accuracy	F1 Score	Accuracy	F1 Score
Statistical	60.28±1.14	59.23±0.97	80.77±0.37	76.72±0.31
Spectral	60.88±1.70	60.53±1.44	78.57±1.46	73.94±0.88
Power	60.15±1.58	59.89±1.75	76.15±2.85	72.91±2.60
Complexity	58.88±2.15	58.28±2.35	69.16±3.59	64.23±3.76
EEGNet	71.91±1.87	71.02±1.82	92.20±0.22	90.25±0.29
TCN	68.71±1.19	68.48±1.29	91.99±0.31	90.08±0.35
MICN	61.46±1.68	61.35±1.69	89.75±0.88	87.80±0.95
TimesNet	61.79±1.79	61.30±1.52	92.31±0.17	90.53±0.21
Autoformer	59.61±2.13	58.88±2.57	88.93±2.64	86.68±2.72
Crossformer	71.90±0.67	71.71±0.62	86.19±0.32	81.61±0.69
FEDformer	60.47±1.60	59.88±1.53	88.53±0.65	86.22±0.79
Informer	61.88±0.99	61.54±1.11	90.78±0.45	88.70±0.51
iTransformer	73.85±0.61	73.47±0.59	79.92±0.37	74.60±0.30
MTST	62.57±2.75	61.41±2.17	78.18±1.04	73.94±0.96
Nonformer	64.28±2.51	63.94±2.42	92.06±0.46	90.20±0.52
PatchTST	59.10±1.08	58.38±1.01	79.47±1.46	75.22±1.25
Pyraformer	66.00±1.49	65.58±1.33	92.51±0.12	90.69±0.14
Reformer	63.45±2.15	61.22±2.23	89.69±0.34	87.19±0.47
Transformer	65.61±2.20	65.19±2.10	91.80±0.29	89.95±0.40
ADformer (Ours)	75.80±0.74	75.19±0.80	94.84±0.19	93.58±0.24

2) *Binary Classification of Large Datasets:* Given the moderate results for the large datasets ADFD and CNBPM

under a subject-independent setup, we investigate whether the presence of an intermediate level of dementia in these datasets makes classification more challenging. To address this, we remove subjects with the intermediate dementia class—frontotemporal Dementia(FTD) in ADFD and Mild Cognitive Impairment(MCI) in CNBPM—resulting in two subsets, ADFD-Binary and CNBPM-Binary, which are more similar to the ADSZ and APAVA datasets. Details of these subsets are shown in Table I. We continue to employ the subject-independent setup to evaluate these two subsets.

The results of our method and all baselines are presented in Table IV. Our method achieves top-1 results in both accuracy and F1 score for these two subsets. Overall, performance significantly improves compared to the three-class classification of the complete datasets, with ADFD-Binary achieving over 70% F1 score and CNBPM-Binary exceeding 90% F1 score with many methods. The higher performance in CNBPM-Binary compared to ADFD-Binary likely results from the larger number of subjects and a relatively balanced distribution of AD and HC subjects. These results do support our guess that some classes of dementia, such as FTD and MCI, are somehow hard to distinguish from AD subjects.

TABLE V: **Subject-Independent: Channel Reduction of Large Datasets.** Following the previous binary classification study of these two datasets, we further investigate how the results are impacted using only 7 channels. Again, we focus only on the Alzheimer’s Disease (AD) and Healthy Controls (HC) subjects, employing the subject-independent setup.

Datasets	ADFD-Binary-7C (2 Classes, 7 Channels) (65 Subjects)		CNBPM-Binary-7C (2 Classes, 7 Channels) (126 Subjects)	
	Accuracy	F1 Score	Accuracy	F1 Score
Statistical	65.61±0.73	64.45±0.65	80.36±0.09	74.95±0.21
Spectral	66.66±0.54	66.12±0.52	79.11±0.28	74.01±0.43
Power	64.59±3.40	63.49±2.64	74.79±4.47	69.36±3.07
Complexity	60.78±2.95	59.58±2.34	66.08±2.65	61.07±2.59
EEGNet	74.69±1.73	73.75±2.18	86.81±2.18	82.96±3.13
TCN	74.87±0.21	74.70±0.19	87.87±0.63	85.62±0.64
MICN	65.47±0.77	65.15±0.64	89.66±0.99	87.45±0.99
TimesNet	70.60±0.23	70.41±0.29	91.16±0.92	89.19±0.89
Autoformer	63.78±1.23	63.41±1.17	85.70±3.56	82.93±4.07
Crossformer	73.87±0.40	73.78±0.35	84.15±0.81	79.01±1.19
FEDformer	65.30±2.32	64.90±2.38	85.66±0.83	82.69±0.81
Informer	67.31±1.02	66.73±0.76	90.53±0.55	88.42±0.62
iTransformer	72.66±0.47	72.22±0.45	76.74±0.58	70.07±0.53
MTST	67.50±0.61	66.97±0.65	77.32±1.63	71.79±1.40
Nonformer	67.52±0.64	67.30±0.52	90.87±0.78	88.61±1.13
PatchTST	65.44±1.23	65.20±1.08	78.35±2.06	72.70±1.46
Pyraformer	72.48±0.52	72.16±0.81	93.48±0.24	91.89±0.33
Reformer	67.65±1.18	64.19±2.45	85.37±1.67	82.22±1.53
Transformer	66.73±0.60	66.50±0.63	90.38±0.36	88.22±0.47
ADformer (Ours)	74.99±0.43	74.72±0.43	92.77±0.30	91.05±0.40

3) *Channel Reduction of Large Datasets:* Considering the relatively poor performance in the Cognision-ERP dataset, we want to investigate whether the fewer channels caused it or if ERP data requires different preprocessing methods from resting EEG data. In this case, we reduce the number of channels used in the ADFD-Binary and CNBPM-Binary datasets to create ADFD-Binary-7C and CNBPM-Binary-7C, respectively.

Specifically, we use only 7 channels—F3, Fz, F4, Cz, P3, Pz, and P4—to match the channels in the Cognision-ERP dataset.

The results of our method and all baselines are presented in Table V. The findings are unexpected yet exciting: the reduced number of channels does not significantly decrease the performance in CNBPM-Binary and even increases the performance in ADFD-Binary. This increase in performance for ADFD-Binary is consistent across nearly all methods, including ours. We verify the results with the validation set and confirm that the improvement is not due to variance in the model on the test set. Performance increased on both validation and test sets. This intriguing result demonstrates that an increased number of channels does not necessarily enhance performance. We suspect the noise introduced in some channels during data collection might be the reason for the lower overall performance. For CNBPM-Binary, the reduced number of channels slightly decreases the overall performance, but the best methods still achieve high performance, with over 90% F1 score.

In summary, reducing the number of channels does not necessarily decrease performance and may even enhance it. This suggests that the poor performance of Cognision-ERP is not solely due to the fewer number of channels but also indicates the need for a specific model design for ERP-EEG data. Moreover, this finding inspires future work on channel selection research. What are the key channels for EEG-based dementia diagnosis? Using fewer channels means cheaper and more convenient EEG devices, making them more applicable to real-world scenarios.

C. Leave-Subjects-Out

This setup is a variant of the subject-independent setup used in many medical settings. It aims to maximize data utilization, especially when dealing with limited sample quality. We randomly select several subjects exclusively for validation and test sets, while the remaining subjects are used for the training set. The preliminary section III-D provides a more detailed discussion of this setup. After the selection, the approximate number of samples across random seeds for ADFD-Binary and CNBPM-Binary is presented in the second tabular of Table I.

1) *Binary Classification of Large Datasets*: We conduct a case study using five seeds (41-45) on the two large datasets with binary classifications: ADFD-Binary and CNBPM-Binary. The results are presented in Table VI. Our method outperforms the baselines on these datasets, achieving F1 scores of 75.22% and 85.19% on ADFD-Binary and CNBPM-Binary, respectively. Compared with the subject-independent setup, the best F1 score for ADFD-Binary remains around 75%, while for CNBPM-Binary, it drops from over 90% to 85%. Both results exhibit very high standard deviations, which is consistent with our expectations. The model is validated on a validation set with fewer subjects, which likely increases the variance introduced by subject-specific noise unrelated to dementia features.

D. Ablation Study

We conduct ablation studies to evaluate different components of our method, including studies on augmentation methods, patch length, target channel numbers, and encoder modules. To

TABLE VI: **Leave-Subjects-Out: Binary-Class Subsets of ADFD and CNBPM.** The leave-subjects-out setup is a specific type of subject-independent setup. This approach randomly selects several subjects for the validation and test sets based on the current random seed and uses all remaining subjects as the training sets. Again, we focus only on the Alzheimer’s Disease (AD) and Healthy Controls (HC) subjects in these datasets.

Datasets	ADFD-Binary (2 Classes, 19 Channels) (65 Subjects)		CNBPM-Binary (2 Classes, 19 Channels) (126 Subjects)	
	Accuracy	F1 Score	Accuracy	F1 Score
Statistical	64.71±4.71	63.55±5.31	73.83±6.78	68.76±7.42
Spectral	64.47±4.57	63.77±4.53	71.72±8.48	68.75±7.47
Power	64.35±2.37	63.45±2.71	69.65±7.47	65.86±7.00
Complexity	58.53±2.04	57.12±2.58	64.84±5.45	60.96±5.21
EEGNet	74.98±4.77	74.62±5.03	85.90±4.35	83.36±4.93
TCN	74.22±6.78	73.97±6.96	86.20±3.85	83.63±3.81
MICN	63.98±5.57	63.48±5.38	80.09±6.53	76.29±8.22
TimesNet	68.10±6.93	67.23±6.99	87.42±4.40	83.96±5.48
Autoformer	66.28±7.04	65.69±7.13	79.26±8.16	72.91±10.03
Crossformer	69.22±5.15	68.78±5.20	80.93±7.70	77.00±6.72
FEDformer	66.52±7.08	65.55±7.89	79.92±7.86	76.62±8.04
Informer	67.90±4.68	67.44±4.62	81.60±7.44	78.58±7.63
iTransformer	71.45±4.19	71.22±4.11	75.61±6.92	71.34±6.85
MTST	63.51±4.43	62.47±4.07	72.76±6.55	67.99±5.67
Nonformer	64.99±4.51	63.46±5.29	81.66±7.72	78.74±7.95
PatchTST	64.29±7.16	63.83±6.92	74.11±7.58	70.23±6.19
Pyraformer	71.72±6.41	70.72±7.88	87.69±4.46	85.15±4.89
Reformer	63.53±4.91	60.16±8.97	79.22±10.45	77.00±9.60
Transformer	62.49±5.14	61.65±5.47	83.18±5.98	80.56±6.68
ADformer (Ours)	75.42±6.06	75.22±6.11	87.52±4.82	85.19±5.61

accurately assess the impact of each component, we select the ADFD-Binary and CNBPM-Binary datasets for evaluation, as they are sufficiently large and have shown good performance in previous studies. In this ablation study, a **default** version of ADformer is defined as employing all augmentation methods, using a patch length list of {1, 2, 4, 8}, a target channel number list of {19, 38, 76, 152}, and enabling inter-granularity self-attention, which may differ from parameters used in previous sections of different setups. The objective here is to assess the effectiveness of each component rather than identifying the best parameters for a dataset. We employ the subject-independent setup for evaluation.

TABLE VII: **Ablation Study: Augmentation Study.** We assess the effectiveness of each augmentation method in our ADformer. The term **All** refers to the collective use of all augmentation methods. We employ the subject-independent setup for evaluation.

Datasets	ADFD-Binary (2 Classes, 19 Channels) (65 Subjects)		CNBPM-Binary (2 Classes, 19 Channels) (126 Subjects)	
	Accuracy	F1 Score	Accuracy	F1 Score
Flip	67.42±3.49	66.98±3.27	93.80±0.73	92.27±0.88
Shuffle	70.53±0.53	69.97±0.81	94.21±0.08	92.81±0.08
Frequency	69.74±2.37	68.91±2.28	93.77±0.24	92.28±0.29
Jitter	68.81±1.37	68.11±1.22	94.84±0.19	93.58±0.24
Drop	66.59±4.12	65.71±3.49	94.14±0.34	92.76±0.40
All	71.03±1.51	70.44±1.35	94.50±0.20	93.15±0.25

1) *Augmentation Study*: We evaluate how different augmentation methods impact the performance of ADFD-Binary and CNBPM-Binary. The results of this augmentation methods study are presented in Table VII. We evaluate each augmentation method described in section IV-B, where the last one **All** refers to using all the methods altogether. The other parameters are the same as a **default** version of ADformer. According to the results, no single augmentation method consistently outperforms the others across both datasets. The best result for ADFD-Binary is achieved using **All**, and for CNBPM-Binary, it is **Jitter**. However, employing all augmentation methods generally yields relatively good performance on both datasets.

TABLE VIII: **Ablation Study: Patch Length Study**. We evaluate how different patch lengths, including single, repetitive, and combinations of patch lengths, impact the performance of ADFD-Binary and CNBPM-Binary. We employ the subject-independent setup for evaluation.

Datasets	ADFD-Binary (2 Classes, 19 Channels) (65 Subjects)		CNBPM-Binary (2 Classes, 19 Channels) (126 Subjects)	
	Accuracy	F1 Score	Accuracy	F1 Score
1	73.61±2.44	73.13±2.58	93.94±0.30	92.43±0.37
2	73.14±0.81	72.85±0.95	94.03±0.34	92.57±0.38
4	74.06±1.74	73.59±1.79	94.26±0.21	92.83±0.25
8	70.95±0.47	70.70±0.52	94.42±0.24	93.01±0.29
1,1,1,1	73.39±0.85	72.98±0.90	94.14±0.24	92.73±0.28
2,2,2,2	71.67±1.66	71.24±1.76	94.12±0.14	92.69±0.16
4,4,4,4	71.77±1.57	71.39±1.71	94.40±0.21	93.05±0.27
8,8,8,8	69.16±1.33	68.69±1.52	94.66±0.29	93.32±0.35
1,2,4,8	71.03±1.51	70.44±1.35	94.50±0.20	93.15±0.25

2) *Patch Length Study*: We evaluate how different patch lengths, including single, repetitive, and combinations of patch lengths, impact the performance of ADFD-Binary and CNBPM-Binary. All other parameters remain consistent with the **default** version of ADformer. The results are presented in Table VIII. The findings indicate that using more patch lengths does not guarantee improved performance. Therefore, the selection of patch lengths should be carefully considered during training. However, analyzing different patch lengths provides valuable insights into which specific lengths are most effective for the current dataset, aiding in the tuning of adaptable parameters.

3) *Channel Number Study*: We evaluate how different target channel numbers, including single, repetitive, and combinations of target channel numbers, impact the performance of ADFD-Binary and CNBPM-Binary. All other parameters align with the **default** version of ADformer. The findings are detailed in Table IX. For CNBPM-Binary, the default version of our method achieves the best performance, while for ADFD-Binary, using four repetitive 19 as target channel numbers yields the best results. These findings echo those from the patch length study, indicating that increasing the number of target channel numbers does not necessarily enhance performance. The results suggest that specific target channel numbers should be selected for different datasets during parameter tuning to optimize performance.

4) *Module Study*: We evaluate how different modules, including data augmentation, inter-granularity self-attention,

TABLE IX: **Ablation Study: Channel Number Study**. We evaluate how different target channel numbers, including single, repetitive, and combinations of channel numbers, impact the performance of ADFD-Binary and CNBPM-Binary. We employ the subject-independent setup for evaluation.

Datasets	ADFD-Binary (2 Classes, 19 Channels) (65 Subjects)		CNBPM-Binary (2 Classes, 19 Channels) (126 Subjects)	
	Accuracy	F1 Score	Accuracy	F1 Score
19	69.41±0.61	68.96±0.66	94.26±0.28	92.88±0.33
38	69.88±1.66	69.42±1.65	94.19±0.20	92.80±0.24
76	70.25±1.82	69.87±1.94	94.17±0.31	92.78±0.35
152	69.98±0.70	69.50±0.76	94.29±0.29	92.88±0.37
19,19,19,19	72.72±1.91	72.35±1.80	94.19±0.32	92.77±0.41
38,38,38,38	70.81±1.70	70.24±1.85	94.17±0.33	92.77±0.40
76,76,76,76	71.14±1.80	70.66±1.79	93.90±0.17	92.40±0.22
152,152,152,152	71.05±1.51	70.48±1.63	94.26±0.13	92.86±0.16
19,38,76,152	71.03±1.51	70.44±1.35	94.50±0.20	93.15±0.25

TABLE X: **Ablation Study: Module Study**. We evaluate how different modules, including data augmentation, inter-granularity self-attention, patch branch, and channel branch, impact the performance of ADFD-Binary and CNBPM-Binary. We employ the subject-independent setup for evaluation.

Datasets	ADFD-Binary (2 Classes, 19 Channels) (65 Subjects)		CNBPM-Binary (2 Classes, 19 Channels) (126 Subjects)	
	Accuracy	F1 Score	Accuracy	F1 Score
No Augmentation	69.21±1.78	68.71±1.78	93.03±0.23	91.37±0.26
No Inter-Attention	69.68±1.51	69.05±1.29	94.34±0.39	92.96±0.47
No Patch Branch	75.09±0.57	74.67±0.62	92.53±0.40	90.61±0.49
No Channel Branch	68.88±0.51	68.38±0.44	93.29±0.12	91.65±0.14
ADformer	71.03±1.51	70.44±1.35	94.50±0.20	93.15±0.25

patch branch, and channel branch, impact the performance of ADFD-Binary and CNBPM-Binary. The patch branch refers to areas b) and d), and the channel branch refers to areas c) and e) in Figure 3, respectively. All other parameters align with the **default** version of ADformer. The findings are detailed in Table X. For CNBPM-Binary, the default version of our method achieves the best performance, underscoring the effectiveness of each component. For ADFD-Binary, our method achieves the best result without the patch branch, significantly outperforming the default version. The other components also contribute positively to the overall results. This outcome aligns with previous findings in Table IV and Table V, where methods that utilize self-attention among channels, such as the iTransformer and Crossformer, demonstrate strong performance on ADFD-Binary and ADFD-Binary-7C. We are unsure of the underlying cause but will investigate this finding in future work.

VII. CONCLUSION AND FUTURE WORKS

A. Conclusion

This paper introduces *ADformer*, a novel multi-granularity transformer designed for EEG-based AD assessment. We develop two innovative multi-granularity data embedding methods to leverage both temporal and spatial features efficiently. The first method embeds cross-channel patches

of varying lengths into multi-granularity embeddings. The second method embeds the series of each channel in inputs transformed with varying numbers of channels into multi-granularity embeddings. Besides, we design two-stage intra-inter granularity self-attention mechanisms to correspond to the two data embedding methods. The intra-granularity self-attention stage leverages local features within each granularity, and the inter-granularity self-attention stage utilizes global features. We evaluate our method comprehensively on 5 complete datasets, totaling 525 subjects, 207,851 samples, and 4 derived subsets of the two largest datasets for case studies. We perform experiments on various setups, including subject-dependent, subject-independent, and leave-subjects-out.

We summarize our key findings from experiments here to inspire the future researchers:

- Deep-learning methods generally outperform traditional feature extraction methods across various setups and datasets. Transformer-based methods, in particular, demonstrate a promising ability to perform EEG-based AD assessment, often achieving comparable or better results than CNN-based methods, especially on large datasets.
- Experiments with the subject-dependent setup consistently achieve much higher results than those with the subject-independent setup. Researchers should avoid using subject-dependent setups to evaluate models in real-world applications, as their deceptively high performance can lead to misleading conclusions.
- Distinguishing between the early stages of Alzheimer’s disease (AD) and other forms of dementia, such as Mild Cognitive Impairment (MCI) and Frontotemporal Dementia (FTD), remains challenging compared to differentiating between Healthy Control (HC) and AD subjects. In a three-class classification involving HC, MCI, and AD, the highest F1 score is around 65%. For binary classification between AD and HC, an EEG dataset with more than 100 subjects collected in a resting state (CNBPM-Binary) can achieve an F1 score of over 90%, even under the challenging subject-independent setup.
- Reducing the number of channels used for training does not necessarily damage the results; sometimes, it even improves them. This is encouraging news for real-world applications, as it suggests the possibility of using cheaper and more convenient EEG helmets. An EEG dataset with more than 100 subjects, utilizing only 7 channels (CNBPM-Binary-7C), achieved F1 scores of around 85%.

B. Future Works

For future work, several directions are promising. Firstly, we aim to explore the importance of channels, determining the minimum number of channels needed to achieve reasonably good results and identifying the most critical channels. Secondly, given that our model and existing methods still exhibit limited performance on EEG-ERP AD data (Cognision-ERP), we plan to investigate effective methods specifically for EEG-ERP data in AD assessment. Thirdly, we intend to develop methods to distinguish between different types of dementia and the early stages of AD more effectively.

From a computer science perspective, designing techniques to learn common features among subjects while ignoring subject-specific noise is crucial in improving classification performance. Considering the limited number of AD datasets, utilizing large pre-trained EEG models might be beneficial. For instance, pre-training on a general EEG dataset and fine-tuning on specific AD and other dementia datasets could be a viable strategy. From a medical perspective, a straightforward approach is to use more advanced and accurate EEG data collectors and to expand data collection across a broader range of subjects.

Acknowledgement We especially thank Dr. Marco Cecchi, Chief Science Officer at Cognision² and a founding member of the ERP Biomarker Qualification Consortium, for his generous help in providing the Cognision-ERP dataset and his valuable suggestions on EEG-based Alzheimer’s Disease assessment. We also appreciate the help of Yu Han, Nan Huang, Taida Li, and Dr. Yujun Yan with data preprocessing, model design, and paper polishing.

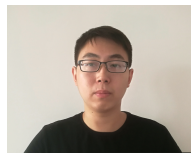
REFERENCES

- [1] World Health Organization. Dementia. <https://www.who.int/news-room/fact-sheets/detail/dementia>, 2023. Created: 15 March 2023.
- [2] Zeinab Breijyeh and Rafik Karaman. Comprehensive review on alzheimer’s disease: Causes and treatment. *Molecules*, 25(24):5789, 2020.
- [3] Colin L Masters, Randall Bateman, Kaj Blennow, Christopher C Rowe, Reisa A Sperling, and Jeffrey L Cummings. Alzheimer’s disease. *Nature reviews disease primers*, 1(1):1–18, 2015.
- [4] Lucy Nelson and Naji Tabet. Slowing the progression of alzheimer’s disease; what works? *Ageing research reviews*, 23:193–209, 2015.
- [5] LW Chu. Alzheimer’s disease: early diagnosis and treatment. *Hong Kong Medical Journal*, 18(3):228, 2012.
- [6] Joon Ho Choi, Hyun-Ah Kim, Wook Kim, Ilhan Lim, Inki Lee, Byung Hyun Byun, Woo Chul Noh, Min-Ki Seong, Seung-Sook Lee, Byung Il Kim, et al. Early prediction of neoadjuvant chemotherapy response for advanced breast cancer using pet/mri image deep learning. *Scientific reports*, 10(1):21149, 2020.
- [7] Claes Nøhr Ladefoged, Lisbeth Marnner, Amalie Hindsholm, Ian Law, Liselotte Højgaard, and Flemming Littrup Andersen. Deep learning based attenuation correction of pet/mri in pediatric brain tumor patients: evaluation in a clinical setting. *Frontiers in neuroscience*, 12:1005, 2019.
- [8] Katerina D Tzamourta, Vasileios Christou, Alexandros T Tzallas, Nikolaos Giannakeas, Loukas G Astrakas, Pantelis Angelidis, Dimitrios Tsalikakis, and Markos G Tsipouras. Machine learning algorithms and statistical approaches for alzheimer’s disease analysis based on resting-state eeg recordings: A systematic review. *International journal of neural systems*, 31(05):2130002, 2021.
- [9] Cosimo Ieracitano, Nadia Mammoni, Alessia Bramanti, Amir Hussain, and Francesco C Morabito. A convolutional neural network approach for classification of dementia stages based on 2d-spectral representation of eeg recordings. *Neurocomputing*, 323:96–107, 2019.
- [10] Xiaotong Gu, Zehong Cao, Alireza Jolfaei, Peng Xu, Dongrui Wu, Tzyy-Ping Jung, and Chin-Teng Lin. Eeg-based brain-computer interfaces (bcis): A survey of recent studies on signal sensing technologies and computational intelligence approaches and their applications. *IEEE/ACM transactions on computational biology and bioinformatics*, 18(5):1645–1666, 2021.
- [11] Katerina D Tzamourta, Nikolaos Giannakeas, Alexandros T Tzallas, Loukas G Astrakas, Theodora Afrantou, Panagiotis Ioannidis, Nikolaos Grigoriadis, Pantelis Angelidis, Dimitrios G Tsalikakis, and Markos G Tsipouras. Eeg window length evaluation for the detection of alzheimer’s disease over different brain regions. *Brain sciences*, 9(4):81, 2019.

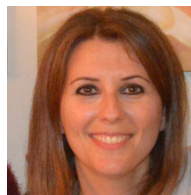
²<https://www.cognision.com/>

- [12] Katerina D Tzamourta, Theodora Afrantou, Panagiotis Ioannidis, Maria Karatzikou, Alexandros T Tzallas, Nikolaos Giannakeas, Loukas G Astrakos, Pantelis Angelidis, Evripidis Glavas, Nikolaos Grigoriadis, et al. Analysis of electroencephalographic signals complexity regarding alzheimer's disease. *Computers & Electrical Engineering*, 76:198–212, 2019.
- [13] Jing Wang, Yuxing Fang, Xiao Wang, Huichao Yang, Xin Yu, and Huali Wang. Enhanced gamma activity and cross-frequency interaction of resting-state electroencephalographic oscillations in patients with alzheimer's disease. *Frontiers in aging neuroscience*, 9:243, 2017.
- [14] Raymundo Cassani, Tiago H Falk, Francisco J Fraga, Paulo AM Kanda, and Renato Anghinah. The effects of automated artifact removal algorithms on electroencephalography-based alzheimer's disease diagnosis. *Frontiers in aging neuroscience*, 6:55, 2014.
- [15] Golshan Fahimi, Seyed Mahmoud Tabatabaei, Elnaz Fahimi, and Hamid Rajebi. Index of theta/alpha ratio of the quantitative electroencephalogram in alzheimer's disease: a case-control study. *Acta Medica Iranica*, pages 502–506, 2017.
- [16] Magali T Schmidt, Paulo AM Kanda, Luis FH Basile, Helder Frederico da Silva Lopes, Regina Baratho, Jose LC Demario, Mario S Jorge, Antonio E Nardi, Sergio Machado, Jéssica N Ianof, et al. Index of alpha/theta ratio of the electroencephalogram: a new marker for alzheimer's disease. *Frontiers in aging neuroscience*, 5:60, 2013.
- [17] Heinrich Garn, Markus Waser, Manfred Deistler, Thomas Benke, Peter Dal-Bianco, Gerhard Ransmayr, Helena Schmidt, Guenter Sanin, Peter Santer, Georg Carvias, et al. Quantitative eeg markers relate to alzheimer's disease severity in the prospective dementia registry austria (prodem). *Clinical Neurophysiology*, 126(3):505–513, 2015.
- [18] Hamed Azami, Steven E Arnold, Saeid Sanei, Zhuoqing Chang, Guillermo Sapiro, Javier Escudero, and Anoopum S Gupta. Multiscale fluctuation-based dispersion entropy and its applications to neurological diseases. *IEEE Access*, 7:68718–68733, 2019.
- [19] Fangzhou Li, Shoya Matsumori, Naohiro Egawa, Shusuke Yoshimoto, Kotaro Yamashiro, Haruo Mizutani, Noriko Uchida, Atsuko Kokuryu, Akira Kuzuya, Ryosuke Kojima, et al. Predictive diagnostic approach to dementia and dementia subtypes using wireless and mobile electroencephalography: A pilot study. *Bioelectricity*, 4(1):3–11, 2022.
- [20] Ozlem Karabiber Cura, Gulce C Yilmaz, H Sabiha Ture, and Aydin Akan. Deep time-frequency feature extraction for alzheimer's dementia eeg classification. In *2022 Medical Technologies Congress (TIPTKNO)*, pages 1–4. IEEE, 2022.
- [21] Xiaocai Shan, Jun Cao, Shoudong Huo, Liangyu Chen, Ptolemaios Georgios Sarrigiannis, and Yifan Zhao. Spatial-temporal graph convolutional network for alzheimer classification based on brain functional connectivity imaging of electroencephalogram. *Human Brain Mapping*, 43(17):5194–5209, 2022.
- [22] Dominik Klepl, Fei He, Min Wu, Daniel J Blackburn, and Ptolemaios Sarrigiannis. Adaptive gated graph convolutional network for explainable diagnosis of alzheimer's disease using eeg data. *IEEE Transactions on Neural Systems and Rehabilitation Engineering*, 2023.
- [23] Andreas Miltioudou, Emmanouil Gionanidis, Katerina D Tzamourta, Nikolaos Giannakeas, and Alexandros T Tzallas. Dice-net: a novel convolution-transformer architecture for alzheimer detection in eeg signals. *IEEE Access*, 2023.
- [24] Yihe Wang, Yu Han, Haishuai Wang, and Xiang Zhang. Contrast everything: A hierarchical contrastive framework for medical time-series. *Advances in Neural Information Processing Systems*, 36, 2023.
- [25] Ashish Vaswani, Noam Shazeer, Niki Parmar, Jakob Uszkoreit, Llion Jones, Aidan N Gomez, Łukasz Kaiser, and Illia Polosukhin. Attention is all you need. *Advances in neural information processing systems*, 30, 2017.
- [26] Haixu Wu, Jiehui Xu, Jianmin Wang, and Mingsheng Long. Autoformer: Decomposition transformers with auto-correlation for long-term series forecasting. *Advances in Neural Information Processing Systems*, 34:22419–22430, 2021.
- [27] Haoyi Zhou, Shanghang Zhang, Jieqi Peng, Shuai Zhang, Jianxin Li, Hui Xiong, and Wancai Zhang. Informer: Beyond efficient transformer for long sequence time-series forecasting. In *Proceedings of the AAAI conference on artificial intelligence*, volume 35, pages 11106–11115, 2021.
- [28] Yong Liu, Tengge Hu, Haoran Zhang, Haixu Wu, Shiyu Wang, Lintao Ma, and Mingsheng Long. itransformer: Inverted transformers are effective for time series forecasting. *International Conference on Learning Representations*, 2024.
- [29] Yuqi Nie, Nam H Nguyen, Phanwadee Sinthong, and Jayant Kalagnanam. A time series is worth 64 words: Long-term forecasting with transformers. *ICLR*, 2023.
- [30] Yunhao Zhang and Junchi Yan. Crossformer: Transformer utilizing cross-dimension dependency for multivariate time series forecasting. In *The Eleventh International Conference on Learning Representations*, 2022.
- [31] NN Kulkarni and VK Bairagi. Extracting salient features for eeg-based diagnosis of alzheimer's disease using support vector machine classifier. *IETE Journal of Research*, 63(1):11–22, 2017.
- [32] Paulo Afonso Medeiros Kanda, Lucas R Trambaiolli, Ana C Lorena, Francisco J Fraga, Luis Fernando I Basile, Ricardo Nitri, and Renato Anghinah. Clinician's road map to wavelet eeg as an alzheimer's disease biomarker. *Clinical EEG and neuroscience*, 45(2):104–112, 2014.
- [33] Markus Waser, Manfred Deistler, Heinrich Garn, Thomas Benke, Peter Dal-Bianco, Gerhard Ransmayr, Dieter Grossegger, and Reinhold Schmidt. Eeg in the diagnostics of alzheimer's disease. *Statistical Papers*, 54:1095–1107, 2013.
- [34] Lucie Tylova, Jaromir Kukal, and Oldrich Vysata. Predictive models in diagnosis of alzheimer's disease from eeg. *Acta Polytechnica*, 53(2), 2013.
- [35] Aldo Mora-Sánchez, Gérard Dreyfus, and François-Benoît Vialatte. Scale-free behaviour and metastable brain-state switching driven by human cognition, an empirical approach. *Cognitive neurodynamics*, 13:437–452, 2019.
- [36] Ruofan Wang, Jiang Wang, Shunan Li, Haitao Yu, Bin Deng, and Xile Wei. Multiple feature extraction and classification of electroencephalograph signal for alzheimers' with spectrum and bispectrum. *Chaos: An Interdisciplinary Journal of Nonlinear Science*, 25(1), 2015.
- [37] Francisco J Fraga, Tiago H Falk, Paulo AM Kanda, and Renato Anghinah. Characterizing alzheimer's disease severity via resting-awake eeg amplitude modulation analysis. *PLoS one*, 8(8):e72240, 2013.
- [38] Luke Tait, George Stothart, Elizabeth Coulthard, Jon T Brown, Nina Kazanina, and Marc Goodfellow. Network substrates of cognitive impairment in alzheimer's disease. *Clinical Neurophysiology*, 130(9):1581–1595, 2019.
- [39] Markus Waser, Heinrich Garn, Reinhold Schmidt, Thomas Benke, Peter Dal-Bianco, Gerhard Ransmayr, Helena Schmidt, Stephan Seiler, Günter Sanin, Florian Mayer, et al. Quantifying synchrony patterns in the eeg of alzheimer's patients with linear and non-linear connectivity markers. *Journal of Neural Transmission*, 123:297–316, 2016.
- [40] Lucas R Trambaiolli, Ana C Lorena, Francisco J Fraga, Paulo AM Kanda, Renato Anghinah, and Ricardo Nitri. Improving alzheimer's disease diagnosis with machine learning techniques. *Clinical EEG and neuroscience*, 42(3):160–165, 2011.
- [41] Xiaokun Liu, Chunlai Zhang, Zheng Ji, Yi Ma, Xiaoming Shang, Qi Zhang, Wencheng Zheng, Xia Li, Jun Gao, Ruofan Wang, et al. Multiple characteristics analysis of alzheimer's electroencephalogram by power spectral density and lempel-ziv complexity. *Cognitive neurodynamics*, 10:121–133, 2016.
- [42] Lucie Tylová, Jaromír Kukal, Václav Hubata-Vacek, and Oldřich Vyšata. Unbiased estimation of permutation entropy in eeg analysis for alzheimer's disease classification. *Biomedical Signal Processing and Control*, 39:424–430, 2018.
- [43] Carmina Coronel, Heinrich Garn, Markus Waser, Manfred Deistler, Thomas Benke, Peter Dal-Bianco, Gerhard Ransmayr, Stephan Seiler, Dieter Grossegger, and Reinhold Schmidt. Quantitative eeg markers of entropy and auto mutual information in relation to mmse scores of probable alzheimer's disease patients. *Entropy*, 19(3):130, 2017.
- [44] Ali H Hussein Al-Nuaimi, Emmanuel Jammeh, Lingfen Sun, and Emmanuel Ifeachor. Complexity measures for quantifying changes in electroencephalogram in alzheimer's disease. *Complexity*, 2018(1):8915079, 2018.
- [45] Yilu Zhao and Lianghua He. Deep learning in the eeg diagnosis of alzheimer's disease. In *Computer Vision-ACCV 2014 Workshops: Singapore, Singapore, November 1-2, 2014, Revised Selected Papers, Part I 12*, pages 340–353. Springer, 2015.
- [46] Mohamed Ismail, Klaus Hofmann, and Mohamed A Abd El Ghany. Early diagnoses of alzheimer using eeg data and deep neural networks classification. In *2019 IEEE Global Conference on Internet of Things (GCIoT)*, pages 1–5. IEEE, 2019.
- [47] Minghao Liu, Shengqi Ren, Siyuan Ma, Jiahui Jiao, Yizhou Chen, Zhiguang Wang, and Wei Song. Gated transformer networks for multivariate time series classification. *arXiv preprint arXiv:2103.14438*, 2021.
- [48] Zekun Li, Shiyang Li, and Xifeng Yan. Time series as images: Vision transformer for irregularly sampled time series. *Advances in Neural Information Processing Systems*, 36, 2024.
- [49] Yihe Wang, Nan Huang, Taida Li, Yujun Yan, and Xiang Zhang. Medformer: A multi-granularity patching transformer for medical time-series classification. *arXiv preprint arXiv:2405.19363*, 2024.

- [50] Junho Song, Keonwoo Kim, Jeonglyul Oh, and Sungzoon Cho. Memento: Memory-guided transformer for multivariate time series anomaly detection. *Advances in Neural Information Processing Systems*, 36, 2024.
- [51] Jiehui Xu, Haixu Wu, Jianmin Wang, and Mingsheng Long. Anomaly transformer: Time series anomaly detection with association discrepancy. *International Conference on Learning Representations*, 2021.
- [52] Shizhan Liu, Hang Yu, Cong Liao, Jianguo Li, Weiyao Lin, Alex X Liu, and Schahram Dustdar. Pyraformer: Low-complexity pyramidal attention for long-range time series modeling and forecasting. In *International conference on learning representations*, 2021.
- [53] Yong Liu, Haixu Wu, Jianmin Wang, and Mingsheng Long. Non-stationary transformers: Exploring the stationarity in time series forecasting. *Advances in Neural Information Processing Systems*, 35:9881–9893, 2022.
- [54] Tian Zhou, Ziqing Ma, Qingsong Wen, Xue Wang, Liang Sun, and Rong Jin. Fedformer: Frequency enhanced decomposed transformer for long-term series forecasting. In *International Conference on Machine Learning*, pages 27268–27286. PMLR, 2022.
- [55] Xue Wang, Tian Zhou, Qingsong Wen, Jinyang Gao, Bolin Ding, and Rong Jin. Card: Channel aligned robust blend transformer for time series forecasting. In *International Conference on Learning Representations*, 2023.
- [56] Peng Chen, Yingying ZHANG, Yunyao Cheng, Yang Shu, Yihang Wang, Qingsong Wen, Bin Yang, and Chenjuan Guo. Pathformer: Multi-scale transformers with adaptive pathways for time series forecasting. In *The Twelfth International Conference on Learning Representations*, 2024.
- [57] Amin Shabani, Amir Abdi, Lili Meng, and Tristan Sylvain. Scaleformer: Iterative multi-scale refining transformers for time series forecasting. *arXiv preprint arXiv:2206.04038*, 2022.
- [58] Joseph Y Cheng, Hanlin Goh, Kaan Dogrusoz, Oncel Tuzel, and Erdrin Azemi. Subject-aware contrastive learning for biosignals. *arXiv preprint arXiv:2007.04871*, 2020.
- [59] Isabela Albuquerque, João Monteiro, Olivier Rosanne, Abhishek Tiwari, Jean-François Gagnon, and Tiago H Falk. Cross-subject statistical shift estimation for generalized electroencephalography-based mental workload assessment. In *2019 IEEE International Conference on Systems, Man and Cybernetics (SMC)*, pages 3647–3653. IEEE, 2019.
- [60] Chaoqi Yang, M Brandon Westover, and Jimeng Sun. Manyd: Many-domain generalization for healthcare applications. In *The Eleventh International Conference on Learning Representations*, 2022.
- [61] Ziyu Liu, Azadeh Alavi, Minyi Li, and Xiang Zhang. Guidelines for augmentation selection in contrastive learning for time series classification. *arXiv preprint arXiv:2407.09336*, 2024.
- [62] Rushuang Zhou, Lei Lu, Zijun Liu, Ting Xiang, Zhen Liang, David A Clifton, Yining Dong, and Yuan-Ting Zhang. Semi-supervised learning for multi-label cardiovascular diseases prediction: a multi-dataset study. *IEEE Transactions on Pattern Analysis and Machine Intelligence*, 2023.
- [63] Xiang Zhang, Ziyuan Zhao, Theodoros Tsiligkaridis, and Marinka Zitnik. Self-supervised contrastive pre-training for time series via time-frequency consistency. *Advances in Neural Information Processing Systems*, 35:3988–4003, 2022.
- [64] Vincent Bazinet, Justine Y Hansen, and Bratislav Mistic. Towards a biologically annotated brain connectome. *Nature reviews neuroscience*, 24(12):747–760, 2023.
- [65] Saeid Sanei and Jonathon A Chambers. *EEG signal processing*. John Wiley & Sons, 2013.
- [66] Selcan Kaplan Berkaya, Alper Kursat Uysal, Efnan Sora Gunal, Semih Ergin, Serkan Gunal, and M Bilginer Gulmezoglu. A survey on eeg analysis. *Biomedical Signal Processing and Control*, 43:216–235, 2018.
- [67] Ting Chen, Simon Kornblith, Mohammad Norouzi, and Geoffrey Hinton. A simple framework for contrastive learning of visual representations. In *International conference on machine learning*, pages 1597–1607. PMLR, 2020.
- [68] Zhihan Yue, Yujing Wang, Juanyong Duan, Tianmeng Yang, Congrui Huang, Yunhai Tong, and Bixiong Xu. Ts2vec: Towards universal representation of time series. In *Proceedings of the AAAI Conference on Artificial Intelligence*, volume 36, pages 8980–8987, 2022.
- [69] Caroline L Alves, Aruane M Pineda, Kirstin Roster, Christiane Thielemann, and Francisco A Rodrigues. Eeg functional connectivity and deep learning for automatic diagnosis of brain disorders: Alzheimer’s disease and schizophrenia. *Journal of Physics: complexity*, 3(2):025001, 2022.
- [70] J Escudero, Daniel Abásolo, Roberto Hornero, Pedro Espino, and Miguel López. Analysis of electroencephalograms in alzheimer’s disease patients with multiscale entropy. *Physiological measurement*, 27(11):1091, 2006.
- [71] Andreas Miltiadous, Katerina D Tzimirta, Theodora Afrantou, Panagiotis Ioannidis, Nikolaos Grigoriadis, Dimitrios G Tsalikakis, Pantelis Angelidis, Markos G Tspirouras, Euripidis Glavas, Nikolaos Giannakeas, et al. A dataset of scalp eeg recordings of alzheimer’s disease, frontotemporal dementia and healthy subjects from routine eeg. *Data*, 8(6):95, 2023.
- [72] Cosimo Ieracitano, Nadia Mammone, Alessia Bramanti, Silvia Marino, Amir Hussain, and Francesco Carlo Morabito. A time-frequency based machine learning system for brain states classification via eeg signal processing. In *2019 International Joint Conference on Neural Networks (IJCNN)*, pages 1–8. IEEE, 2019.
- [73] Juan P Amezcua-Sanchez, Nadia Mammone, Francesco C Morabito, Silvia Marino, and Hojjat Adeli. A novel methodology for automated differential diagnosis of mild cognitive impairment and the alzheimer’s disease using eeg signals. *Journal of neuroscience methods*, 322:88–95, 2019.
- [74] Marco Cecchi, Dennis K Moore, Carl H Sadowsky, Paul R Solomon, P Murali Doraiswamy, Charles D Smith, Gregory A Jicha, Andrew E Budson, Steven E Arnold, and Kalford C Fadem. A clinical trial to validate event-related potential markers of alzheimer’s disease in outpatient settings. *Alzheimer’s & Dementia: Diagnosis, Assessment & Disease Monitoring*, 1(4):387–394, 2015.
- [75] Vernon J Lawhern, Amelia J Solon, Nicholas R Waytowich, Stephen M Gordon, Chou P Hung, and Brent J Lance. Eegnet: a compact convolutional neural network for eeg-based brain-computer interfaces. *Journal of neural engineering*, 15(5):056013, 2018.
- [76] Shaojie Bai, J Zico Kolter, and Vladlen Koltun. An empirical evaluation of generic convolutional and recurrent networks for sequence modeling. *arXiv preprint arXiv:1803.01271*, 2018.
- [77] Huiqiang Wang, Jian Peng, Feihu Huang, Jince Wang, Junhui Chen, and Yifei Xiao. Micn: Multi-scale local and global context modeling for long-term series forecasting. In *The Eleventh International Conference on Learning Representations*, 2022.
- [78] Haixu Wu, Tengge Hu, Yong Liu, Hang Zhou, Jianmin Wang, and Mingsheng Long. Timesnet: Temporal 2d-variation modeling for general time series analysis. In *The eleventh international conference on learning representations*, 2022.
- [79] Yitian Zhang, Liheng Ma, Soumyasundar Pal, Yingxue Zhang, and Mark Coates. Multi-resolution time-series transformer for long-term forecasting. In *International Conference on Artificial Intelligence and Statistics*, pages 4222–4230. PMLR, 2024.
- [80] Nikita Kitaev, Lukasz Kaiser, and Anselm Levskaya. Reformer: The efficient transformer. In *International Conference on Learning Representations*, 2019.
- [81] Pavel Izmailov, Dmitrii Podoprikin, Timur Garipov, Dmitry Vetrov, and Andrew Gordon Wilson. Averaging weights leads to wider optima and better generalization. *arXiv preprint arXiv:1803.05407*, 2018.



Yihe Wang is a Ph.D. student in the Department of Computer Science at the University of North Carolina(UNC) - Charlotte, North Carolina, USA. Yihe received his Bachelor’s degree in Electrical and Computer Engineering from the University of Missouri-Columbia and his Master’s degree in Computer Science from New York University. His research interests lie in time series, self-supervised learning, contrastive learning, and machine learning for healthcare.



Nadia Mammone received the Laurea degree (M.S. equivalent) in electronic engineering and the Ph.D. degree in informatics, biomedical, and telecommunications engineering from the Mediterranean University of Reggio Calabria, in 2003 and 2007, respectively, with a dissertation that was awarded the Caianiello Prize from the Italian Neural Networks Society (SIREN). She is currently an Associate Professor with the DICEAM Department at the University Mediterranea of Reggio Calabria, Italy.



Darina Petrovsky received her PhD in Nursing from the University of Pennsylvania in 2017. Prior to her doctoral work, she received a Masters in Nursing from Case Western Reserve University (2011) and a Bachelor of Musical Arts from the University of Michigan (2009). She is currently an Assistant Professor at Duke University School of Nursing, North Carolina, USA.



Alexandros Tzallas is currently an Associate Professor in the field of Biomedical Engineering and specifically in the “Analysis and Processing of Biomedical Data” at the Department of Informatics and Telecommunications of the University of Ioannina, Greece. He is also affiliated as an Honorary Research Fellow at the Department of Metabolism of Digestion and Reproduction at the Faculty of Medicine of Imperial College London.



Francesco C. Morabito (Senior Member, IEEE) is currently a Full Professor of electrical engineering and neural engineering with the University Mediterranea of Reggio Calabria, Italy. He has served as the Dean of the Faculty of Engineering, from 2001 to 2008, a Vice-Rector for Internationalization from 2013 to 2022, and the Deputy Rector from 2017 to 2018. He has authored or coauthored over 400 papers in international journals/conference proceedings in various fields of engineering (machine/deep learning, biomedical signal processing, radar data processing, nuclear fusion, nondestructive testing and evaluation, and computational intelligence). He has coauthored less than 20 international books (mostly focused on neural networks and machine learning) and held five international patents.



Xiang Zhang is currently an Assistant Professor in the Department of Computer Science at the University of North Carolina (UNC) at Charlotte, North Carolina, USA. Before joining UNC Charlotte, he was a postdoctoral fellow at Harvard University from March 2020 to July 2022. Xiang received his Ph.D. degree (in 2020) in Computer Science from the University of New South Wales (UNSW). His research interests lie in data mining and machine learning with applications in pervasive healthcare, medical time series, and Brain-Computer Interfaces.

SUPPLEMENTARY MATERIAL

S.I. DATASET DETAILS

A. ADSZ

The Alzheimer’s Disease and Schizophrenia (ADSZ) is a public EEG time series dataset³ from paper [69]. We only use the sub-dataset for Alzheimer’s disease(AD) in the download link. The AD sub-dataset is a 2-classes EEG time series dataset of 48 subjects, 24 AD patients, and 24 healthy elderly subjects. It has 19 channels and a sampling frequency rate of 128Hz. Most subjects have an EEG trial duration of 8 seconds, and several trials have 10, 12, or 14 seconds, with timestamps ranging from 1,024 to 1,792. By segmenting each trial into 1-second samples with half-overlapping, we obtain a total of 768 samples with 128 timestamps per sample.

B. APAVA

The Alzheimer’s Patients’ Relatives Association of Valladolid (APAVA) dataset⁴, referenced in the study by [70], is a public 2-classes EEG time series dataset consisting of 23 subjects, including 12 AD patients and 11 healthy elderly subjects. It has 16 channels and a sampling frequency rate of 256Hz. Each subject has multiple trials, with each trial lasting 5 seconds, corresponding to 1280 timestamps. We segment all the trials into 1-second samples with half-overlapping, generating a total of 5,967 samples.

C. ADFD

The Alzheimer’s Disease and Frontotemporal Dementia(ADFD) is a large public 3-classes EEG time series dataset⁵ from the paper [71]. Here, we use data version 1.06. It has 88 subjects, including 36 AD patients, 23 Frontotemporal Dementia (FTD), and 29 healthy controls(HC). It has 19 channels and a sampling frequency rate of 500 Hz. Each subject has a trial, with trials lasting approximately 13.5 minutes for AD subjects (min=5.1, max=21.3), 12 minutes for FTD subjects (min=7.9, max=16.9), and 13.8 for HC subjects (min=12.5, max=16.5). In total, the dataset includes 485.5 minutes of AD, 276.5 minutes of FTD, and 402 minutes of HC time series recordings. A bandpass filtering between 0.5-45Hz is applied to each trial. We downsample each trial into 256Hz and segment them into 1-second non-overlapping samples, discarding any samples shorter than 1 second at the trial edges. This process results in a total of 69,752 samples.

D. ADFD-Binary & ADFD-Binary-7C

These two datasets are subsets of the processed ADFD dataset. The ADFD-Binary dataset excludes all subjects with Frontotemporal Dementia (FTD), resulting in 65 subjects and a total of 53,182 samples. The ADFD-Binary-7C dataset is further processed from the ADFD-Binary dataset by using only 7 channels. These channels include F3, Fz, F4, Cz, P3, Pz, and P4.

³https://figshare.com/articles/dataset/Alzheimer_s_disease_and_Schizophrenia/19091771

⁴<https://osf.io/jbysn/>

⁵<https://openneuro.org/datasets/ds004504/versions/1.0.6>

E. CNBPM

This is a large private 3-classes dataset of preprocessed EEG time series provided by AI-LAB laboratory (University Mediteranea of Reggio Calabria, Italy), referenced in studies [72], [73]. It consists of 63 subjects with Alzheimer’s Disease (AD), 63 with Mild Cognitive Impairment (MCI), and 63 Healthy Control (HC) subjects. The dataset has 19 channels and an initial sampling rate of 1024Hz. A frequency-band filter and downsampling are applied to filter the frequency bands between 0.5 and 32 Hz and reduce the sampling rate to 256Hz. Each subject’s trial, ranging from several minutes to over half an hour, is segmented into 1-second non-overlapping samples, excluding those shorter than 1 second at the trial edges. This procedure yields a total of 70,064 samples.

F. CNBPM-Binary & CNBPM-Binary-7C

Like ADFD-Binary and ADFD-Binary-7C datasets, CNBPM-Binary and CNBPM-Binary-7C are two subsets of the processed ADFD dataset. The CNBPM-Binary dataset excludes all subjects with Mild Cognitive Impairment (MCI), resulting in 126 subjects and a total of 46,305 samples. The CNBPM-Binary-7C dataset is further processed from the CNBPM-Binary dataset by using only 7 channels. These channels include F3, Fz, F4, Cz, P3, Pz, and P4.

G. Cognision-ERP

The Cognision-ERP is a private Event-Related Potential(ERP) EEG time series dataset from *Cognision*⁶ company, referenced in study [74]. It has 177 available subjects, with 90 AD and 87 HC. The total number of samples is 61,300. Each subject has 300 or 400 samples, and each sample has 149 timestamps. The frequency sampling rate is 125Hz, and the channel number is 7.

S.II. IMPLEMENTATION DETAILS

All CNN and transformer-based methods are implemented based on the Time-Series-Library GitHub project⁷. All traditional methods are manually implemented, and training is done under the same framework as deep-learning methods. We use accuracy, macro-averaged F1 score, macro-averaged AUROC, and macro-averaged AUPRC as evaluation metrics. For all the setups, we save the model with the best F1 score on the validation set and test it on the test set to get the final result. Experiments are conducted using five different seeds (41-45) based on the same train-val-test data split in subject-dependent/subject-independent setups and different train-val-test data split in the leave-subjects-out setup, with results reported as mean and standard deviation. Half of the experiments are performed on NVIDIA RTX 4090, and the other half that require more CUDA memory are run on a cluster with four RTX A5000 GPUs. We employ 6 layers for the encoder of all transformer methods, with the self-attention dimension D set to 128 and the hidden dimension of the feed-forward networks set to 256. The optimizer used

⁶<https://www.cognision.com/>

⁷<https://github.com/thuml/Time-Series-Library>

TABLE S.1: **Parameters Tuning.** Parameter tuning for all evaluations of our ADformer model, where the symbol – indicates that a parameter is disabled, and ✓ indicates that it is enabled.

Paras	patch_length_list	channel_number_list	augmentations	no_temporal_branch	no_channel_branch	swa
Subject-Dependent						
ADSZ	{2}	{19}	none,flip0.8	–	–	–
APAVA	{4, 8}	{32, 6}	none,flip0.8	–	–	–
ADFD	{1, 2, 4}	{19, 38}	flip,drop0.25	–	–	–
CNBPM	{2, 2, 2, 4, 4, 4}	{19, 38, 76, 152}	flip,jitter0.25,drop0.25	–	–	–
Cognision-ERP	{3, 3}	–	flip,shuffle	–	✓	–
Subject-Independent						
ADSZ	{4}	{19}	none,drop	–	–	–
APAVA	{2, 2, 4, 16, 32}	{16, 32, 64, 128}	none,drop0.15	–	–	✓
ADFD	{2, 2, 2, 4, 4, 4}	{16, 32, 64, 128}	flip,jitter0.25,drop0.25	–	–	✓
ADFD-Binary	{4}	{19, 19, 19, 19}	flip1.0,shuffle1.0,frequency0.1,jitter0.4,drop0.4	–	–	✓
ADFD-Binary-7C	{2, 2, 2, 4, 4, 4}	{19, 38, 76, 152}	flip1.0,shuffle1.0,frequency0.1,jitter0.3,drop0.3	–	–	✓
CNBPM	{1, 1, 2, 2, 2}	{19, 38, 38, 38, 76}	flip1.0,shuffle1.0,drop0.25	–	–	✓
CNBPM-Binary	{1, 2, 4, 8}	{19, 38, 76, 152}	jitter	–	–	✓
CNBPM-Binary-7C	{1, 2, 2}	{7, 14, 28}	flip1.0,shuffle1.0,jitter0.25,drop0.25	–	–	✓
Cognision-ERP	–	{7, 7}	flip,shuffle	✓	–	✓
Leave-Subjects-Out						
ADFD-Binary	–	{19, 19}	flip,shuffle,frequency,jitter	✓	–	✓
CNBPM-Binary	{6, 6, 8, 8}	{19, 38, 76, 152}	flip,shuffle,jitter,drop	–	–	✓

is Adam, with a learning rate of $1e-4$. Stochastic weight averaging (SWA) [81] is enabled in subject-independent and leave-subjects-out setups to benefit cross-subjects learning. Batch size is set to $\{32, 32, 128, 128, 32\}$ to ADSZ, APAVA, ADFD, CNBPM, and Cognision-ERP, respectively.

Statistical Statistical features are manually extracted from both the raw data and five frequency bands (delta, theta, alpha, beta, gamma), including mean, skewness, kurtosis, standard deviation, interquartile range, maximum, minimum, and median [11], [12], [31]–[35]. A linear projector is then trained on these extracted features.

Spectral Spectral features are manually extracted from the raw data, including Phase Shift, Phase Coherence, Bispectrum, Bicoherence, Spectral Centroid, Spectral Roll-off, Spectral Peak, Average Magnitude, Median Frequency, and Amplitude Modulation [13], [14], [36]–[40]. A linear projector is then trained on these extracted features.

Power Power features are manually extracted from the raw data, including Power Spectrum Density, Relative Band Power, Ratio of EEG Rhythm, and Energy [15], [16], [32], [41]. A linear projector is then trained on these extracted features.

Complexity Complexity features are manually extracted from the raw data, including Shannon entropy, Tsallis Entropy, Permutation Entropy, Spectral Entropy, Bispectral Entropy, and Dispersion entropy [17], [18], [42]–[44]. A linear projector is then trained on these extracted features.

EEGNet EEGNet [75] utilizes 2D convolutional networks to extract temporal and spatial features. Specifically, it employs a temporal convolutional layer, followed by a depthwise convolutional layer, and then a separable convolutional layer to sequentially learn a representation. A linear projector is subsequently trained on this representation.

TCN TCN [76] is a CNN-based method specifically designed for time series data. It uses multi-layer causal dilated 1D convolutional blocks to expand the receptive field of convolutional networks, enabling more effective representation learning on time series data.

MICN MICN [77] introduces a convolutional structure with linear computational complexity for time series forecasting. It employs a local-global structure to achieve information aggregation and model long-term dependencies in time series, outperforming both the self-attention family and auto-correlation mechanisms. The raw source code is available at <https://github.com/wanghq21/MICN>.

TimesNet TimesNet [78] transforms 1D time series data into a 2D space, allowing for the simultaneous presentation of intraperiod and interperiod variations. The authors introduce TimesBlock, a parameter-efficient inception block designed to uncover multiple periods and capture temporal 2D variations from the transformed 2D tensors. The top-k amplitude value is set to 1. The raw code is available at <https://github.com/thuml/Time-Series-Library>.

Autoformer Autoformer [26] employs an auto-correlation mechanism to replace self-attention for time series forecasting. Additionally, they use a time series decomposition block to separate the time series into trend-cyclical and seasonal components for improved learning. The raw source code is available at <https://github.com/thuml/Autoformer>.

Crossformer Crossformer [30] designs a single-channel patching approach for token embedding. They utilize two-stage self-attention to leverage both temporal features and channel correlations. A router mechanism is proposed to reduce time and space complexity during the cross-dimension stage. The raw code is available at <https://github.com/Thinklab-SJTU/Crossformer>.

FEDformer FEDformer [54] leverages frequency domain information using the Fourier transform. They introduce frequency-enhanced blocks and frequency-enhanced attention, which are computed in the frequency domain. A novel time series decomposition method replaces the layer norm module in the transformer architecture to improve learning. The raw code is available at <https://github.com/MAZiqing/FEDformer>.

Informer Informer [27] is the first paper to employ a one-forward procedure instead of an autoregressive method in

time series forecasting tasks. They introduce ProbSparse self-attention to reduce complexity and memory usage. The raw code is available at <https://github.com/zhouhaoyi/Informer2020>.

iTransformer iTransformer [28] questions the conventional approach of embedding attention tokens in time series forecasting tasks and proposes an inverted approach by embedding the whole series of channels into a token. They also invert the dimension of other transformer modules, such as the layer norm and feed-forward networks. The raw code is available at <https://github.com/thuml/iTransformer>.

MTST MTST [79] uses the same token embedding method as Crossformer and PatchTST. It highlights the importance of different patching lengths in forecasting tasks and designs a method that can take different sizes of patch tokens as input simultaneously. The patch length list is set to $\{8, 32, 96\}$. The raw code is available at <https://github.com/networkslab/MTST>.

Nonformer Nonformer [53] analyzes the impact of non-stationarity in time series forecasting tasks and its significant effect on results. They design a de-stationary attention module and incorporate normalization and denormalization steps before and after training to alleviate the over-stationarization problem. The raw code is available at https://github.com/thuml/Nonstationary_Transformers.

PatchTST PatchTST [29] embeds a sequence of single-channel timestamps as a patch token to replace the attention token used in the vanilla transformer. This approach enlarges the receptive field and enhances forecasting ability. The patch length is set to 16. The raw code is available at <https://github.com/yuqinie98/PatchTST>.

Pyraformer Pyraformer [52] captures temporal dependencies across different ranges in a compact, multi-resolution manner. It achieves a maximum path length of $O(1)$ while maintaining the time and space complexity of $O(L)$. The raw code is available at <https://github.com/alipay/Pyraformer>.

Reformer Reformer [80] replaces dot-product attention with locality-sensitive hashing. They also use a reversible residual layer instead of standard residuals. The raw code is available at <https://github.com/lucidrains/reformer-pytorch>.

Transformer Transformer [25], commonly known as the vanilla transformer, is introduced in the well-known paper "Attention is All You Need." It can also be applied to time series by embedding each timestamp of all channels as an attention token. The PyTorch version of the code is available at <https://github.com/jadore801120/attention-is-all-you-need-pytorch>.

ADformer Table S.1 presents the parameter tuning for all evaluations across different datasets and various setups of our ADformer.